Energy & Environmental Science

ROYAL SOCIETY OF CHEMISTRY

PERSPECTIVE

View Article Online
View Journal | View Issue

Cite this: *Energy Environ. Sci.*, 2023, **16**, 1964

A practical perspective on the potential of rechargeable Mg batteries†

J. Alberto Blázquez, *[a] Rudi R. Maça,[a] Olatz Leonet,[a] Eneko Azaceta,[a] Ayan Mukherjee,[b] Zhirong Zhao-Karger,[cd] Zhenyou Li,[cd] Aleksey Kovalevsky,[e] Ana Fernández-Barquín,[a] Aroa R. Mainar,[a] Piotr Jankowski,[f] Laurin Rademacher,[g] Sunita Dey,[h] Siân E. Dutton,[i] Clare P. Grey,[h] Janina Drews,[g] Joachim Häcker,[g] Timo Danner,[cg] Arnulf Latz,[cgj] Dane Sotta,[k] M. Rosa Palacin,[l] Jean-Frédéric Martin,[k] Juan Maria García Lastra,[f] Maximilian Fichtner,[cd] Sumana Kundu,[mn] Alexander Kraytsberg,[mn] Yair Ein-Eli,[mn] Malachi Noked *[b] and Doron Aurbach *[b]

Received 22nd December 2022,
Accepted 8th March 2023

DOI: 10.1039/d2ee04121a

rsc.li/ees

Emerging energy storage systems based on abundant and cost-effective materials are key to overcome the global energy and climate crisis of the 21st century. Rechargeable Magnesium Batteries (RMB), based on Earth-abundant magnesium, can provide a cheap and environmentally responsible alternative to the benchmark Li-ion technology, especially for large energy storage applications. Currently, RMB technology is the subject of intense research efforts at laboratory scale. However, these emerging approaches must be placed in a real-world perspective to ensure that they satisfy key technological requirements. In an attempt to bridge the gap between laboratory advancements and industrial development demands, herein, we report the first non-aqueous multilayer RMB pouch cell prototypes and propose a roadmap for a new advanced RMB chemistry. Through this work, we aim to show the great unrealized potential of RMBs.

Broader context

Today Li-ion batteries (LIBs) are considered the battery technology of reference for many current and promising applications such as transport electrification or renewable energy storage. Despite the good performances of LIBs, they are expected to face resource supply-chain challenges due to the relatively low natural abundancy of lithium (Li) and the geographically uneven distribution worldwide. Shifting towards fully non-Li rechargeable batteries may open an effective way to overcome such challenges. Rechargeable magnesium batteries (RMBs) constitute a paradigmatic example of such promising, alternative non-Li energy storage systems, following pioneering efforts and breakthroughs from world-wide research teams. The potential to use metallic Mg anodes in rechargeable batteries brings important advantages in terms of energy density, cost, safety, sustainability, and lower material supply risk due to the natural abundancy of Mg. Despite the important advances in the RMB literature, all the reported studies are still limited to the laboratory scale and coin-cell configuration, where many practical and industrial aspects of RMB are neglected. In this context, pouch cell configuration is a better platform to optimize components, and it represents a crucial step towards an application ready battery cell design. Herein, in this paper we present a critical perspective of the most promising materials and cell components for the development of high-TRL RMBs with competitive performances. The feasibility and great untapped potential of possible advanced RMB chemistry is highlighted. A roadmap for the development of mature RMBs that can reach an energy density of up to 160 W h kg^{-1} is outlined.

[a] *CIDETEC, Basque Research and Technology Alliance (BRTA), Parque Científico y Tecnológico de Gipuzkoa, Paseo Miramón, 196, 20014, Donostia-San Sebastián, Spain. E-mail: ablazquez@cidetec.es*
[b] *Department of Chemistry, Bar Ilan University, Ramat Gan, 5290002, Israel*
[c] *Helmholtz Institute Ulm (HIU) Electrochemical Energy Storage, D-89081, Ulm, Germany*
[d] *Institute of Nanotechnology (INT), Karlsruhe Institute of Technology (KIT), D-76021, Karlsruhe, Germany*
[e] *Israel Institute of Metals, Technion R&D foundation LTD., Technion City, Haifa, 3200003, Israel*
[f] *Department of Energy Conversion and Storage, Technical University of Denmark, Kgs. Lyngby, Denmark*
[g] *Institute of Engineering Thermodynamics, German Aerospace Center (DLR), Pfaffenwaldring 38-40, D-70569, Stuttgart, Germany*
[h] *Department of Chemistry, University of Cambridge, Cambridge CB2 1EW, UK*
[i] *Cavendish Laboratory, University of Cambridge, JJ Thomson Avenue, Cambridge, CB3 0HE, UK*
[j] *Institute of Electrochemistry, Ulm University, D-89081, Ulm, Germany*
[k] *CEA-LITEN, 17 Rue des Martyrs, 38054 Grenoble Cedex 9, France*
[l] *Institut de Ciéncia de Materials de Barcelona, ICMAB-CSIC, Campus de la UAB, 08193 Bellaterra, Catalonia, Spain*
[m] *Department of Materials Science and Engineering, Technion-Israel Institute of Technology, Haifa, 3200003, Israel*
[n] *Grand Technion Energy Program (GTEP), Technion-Israel Institute of Technology, Haifa, 3200003, Israel*

† Electronic supplementary information (ESI) available. See DOI: https://doi.org/10.1039/d2ee04121a

1. Introduction

Over the last decade, the growing markets of zero-emission electromobility, large-scale stationary storage for renewable energy production, and portable consumer electronics have increased the demand for Li-ion battery cells exponentially, and they are forecasted to do so for at least another decade.[1] This unsustainable growth is predicted to cause cell shortages due to severe Li-ion battery raw-material bottlenecks, especially lithium, nickel, and cobalt, owing to their limited amount, uneven geopolitical distribution (particularly Co), and the lack of political stability of some of the countries mining the resources.[2,3] Therefore, even old chemistries with moderate to poor performance, such as lead–acid batteries, are being considered as an alternative for stationary applications, to relieve the pressure on the electromobility market.[4]

In this context, the emergence of environmentally friendly battery technologies made of abundant, low-cost materials incurring low supply risk and exhibiting high energy density and performance is direly needed to achieve the set climate change goals.[5–7] Rechargeable magnesium batteries (RMBs) are a very promising battery technology candidate on account of the high specific capacity (2205 mA h g^{-1}), high volumetric capacity (3832 mA h cm^{-3}), and low reduction potential (−2.37 V *vs.* SHE) of magnesium.[8–10] Moreover, magnesium is the 8th most abundant element in the Earth's crust, is non-toxic and safe for handling in ambient air, has a low atomic weight, and is less inclined than other metals to dendrite formation during plating/stripping reactions,[7,11–13] despite more recently the electrochemical growth of fractal Mg dendrites from Grignard reagents has been observed in symmetric cells.[14] Additionally, in terms of the environmental friendliness of the entire supply chain, recycling reduces the demand for primary magnesium by up to 50%, unlike currently impractical lithium recycling (<1%).[15,16] Although the feasibility of RMB was demonstrated at the laboratory scale by Aurbach's group in 2000,[17] its low technology readiness level (TRL) (1–3)[18] is still one of its major drawbacks, mainly because of challenges related to the lack of high-TRL electrolyte solutions and intercalation compounds. Since then, the scientific community has been focused on Li-ion battery research, with limited attention to divalent alternatives. Nowadays, the raised awareness of the limitations of lithium-ion batteries and growing market demand have led to an increase in the number of studies and intellectual property rights (IPR) petitions related to RMB components among alternative chemistries (Fig. 1). For the sake of comparison, the number of publications regarding lithium batteries has been included in the ESI† (Fig. SI1). Despite these developments, studies have still been limited to the laboratory scale and based on the coin-cells configuration, where many practical and industrial aspects of RMB are neglected. In this context, the pouch cells configuration is a better platform to optimize components, and it represents a crucial step towards an application-ready battery. Besides, large scale Mg-metal batteries have the potential to be integrated in a simpler battery packs (BP) reducing the cost and their

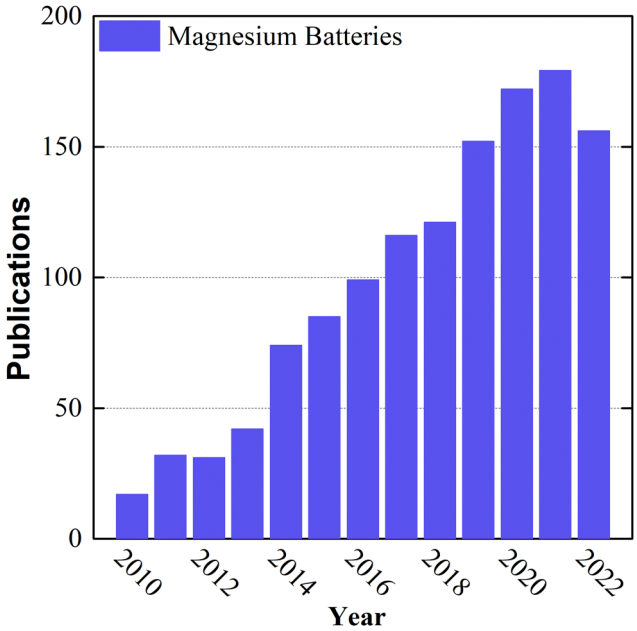

Fig. 1 Number of publications per year, including the words "magnesium batteries" in their title, during the last two decades, based on data taken from the Web of Science.

production will demand a greener infrastructure. Additionally, this novel technology could be manufactured using the actual LIB production lines[19,20] The conventional state-of-the-art RMB model, utilizes a thick (100 μm) pure magnesium metal anode, a Chevrel-phase (CP) Mo_6S_8 cathode on a nickel current collector, and an "all phenyl complex" (APC) electrolyte solution consisting of phenylmagnesium chloride (C_6H_5MgCl), aluminum chloride ($AlCl_3$), and tetrahydrofuran (THF). In this system, the components are fairly compatible with each other and able to provide practical capacities of up to 70 mA h g_{CP}^{-1} in the laboratory-scale coin cell configuration without side reactions.[21] Although this system is functional, to the best of our knowledge, the technology has never been adapted to a larger size pouch cell configuration for cell optimization toward industrial use; this is due to the various disadvantages of each component, which are not suitable for mass production or are not economically viable.

Herein, we present a critical perspective of the most promising materials and cell components for the development of high-TRL RMB which we have evaluated their potential in industrial-level battery cells. Xiu *et al.*[22] have reported previously single layer Mg-based pouch cells, but with the same format as coin cells. However, in the perspective work described herein, for the first time, magnesium batteries were tested in real pouch cell prototypes comprising conventional pure Mg metal-foil anodes, APC electrolyte solution and CP cathodes in an effort to demonstrate an RMB at a high TRL. The differences between pouch cell format and lab-scale coin cell components were explained, and the impact on energy and mass was calculated. Finally, the impact of some of the most novel materials reported in the literature, such as a thin foil of magnesium alloy AZ31, a $Mg[B(hfip)_4]_2$/DME electrolyte

solution, and the VS_4 cathode active material was examined. The latter may enable RMB having a much higher energy density than the first generation, which is based on CP cathodes. The feasibility and great untapped potential of possible advanced RMB chemistry is highlighted. A roadmap for the development of mature RMB that can reach an energy density of up to 150 W h kg^{-1} is outlined.

2. Electrolytes

The electrolytes are arguably one of the most important components in a battery because of their continuous contact with all the cell components. An ideal electrolyte solution has high thermal, chemical, and electrochemical stability, allowing efficient reversible magnesium plating/stripping and ion diffusion. Importantly, for the Mg electrodes to exhibit a fully reversible behavior, no side reactions must occur. In contrast to the case of the Li- and Na-metal anodes, on which surface films formed by side reactions may behave like solid electrolyte interphases (the SEI model), any such surface film formed on Mg electrodes is prone to block the ion flow, leading to their deactivation. "All phenyl complex" APC electrolyte solutions, developed more than two decades ago,[23] are nowadays among the most widely used solutions in the RMB field. They comprise the reaction products of Lewis base C_6H_5MgCl with Lewis acid $AlCl_3$ in THF; due to the *trans*-metalation reaction between the Al and Mg cores, which exchange ligands, complex solutions containing $MgCl(THF)_5^+$ cations and $AlCl_x(C_6H_5)_{4-x}^-$ anions are formed. These solutions allow the fully reversible deposition/dissolution of Mg and exhibit wide electrochemical windows (> 3 V) (Fig. 2).

The starting point in the search for suitable Mg electrolytes were Grignard reagent solutions comprising RMgX (X = Cl, Br) or MgR_2 Lewis bases and ethereal solvents like THF. Building on these foundations, the first milestones on the way to advanced APC electrolyte solutions were the development of $Mg(BR_4)_2$ ether solutions containing organo–borate anions by Gregory *et al.*[24] and the development of organo–chloro–aluminate anions $Mg(AlCl_xR_{4-x})_2$ complexes by Aurbach *et al.*,[7] (where R is an organic group, such as methyl, ethyl, and butyl). The next step was to use ethereal solutions containing products of reactions between Grignard Lewis bases and Lewis acids, such as $AlCl_3$ or $AlCl_xR_{3-x}$.[25] These electrolyte solutions, containing organo–halo–aluminate Mg salts such as $Mg(AlCl_3R)_2$ and $Mg(AlCl_2RR')_2$, demonstrate a room-temperature conductivity comparable to that of Li salts solutions at moderate salt concentrations (0.3–0.5 M) in THF or polyether solvents. Mixing Bu_2Mg and $EtAlCl_2$ in THF in a 1 : 2 molar ratio afforded the best-performing solution, having an ionic conductivity of 1.4 mS cm^{-1} and anodic stability up to 2.2 V; it was later called the dichloro complex (DCC).[17,25,26] However, even the best DCC electrolyte solution does not satisfy the requirements of high voltage, high-energy RMB applications for a wide electrochemical stability window (> 3.5 V), chemical stability, and safety.[27] During studies on advanced Grignard-based electrolyte

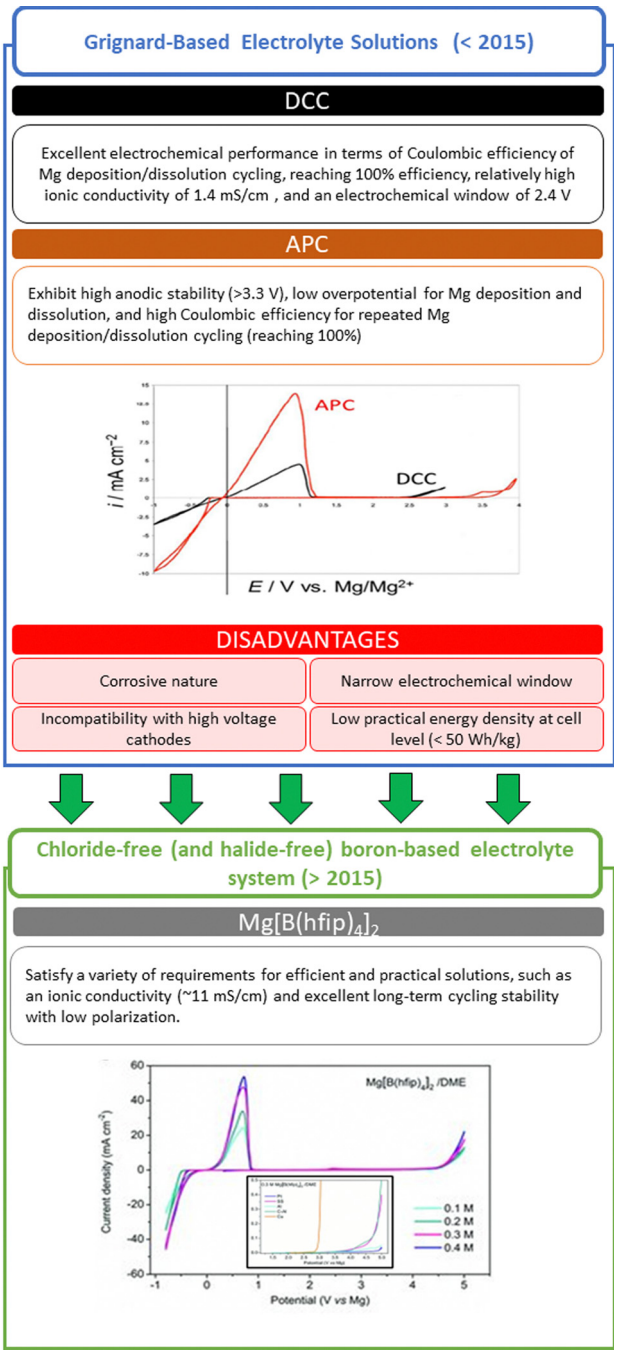

Fig. 2 Summary and evolution of electrolyte solutions.[3,35]

solutions, it was understood that β-H elimination reaction, that is, the elimination of a hydrogen attached to a β-carbon (the second carbon of an alkyl ligand bound to the metal center), was the cause of the limited electrochemical window. In advanced Grignard-based electrolyte solutions such as APC, the organic ligand phenyl is directly bonded to a magnesium atom (*e.g.*, PhMgCl) and no hydrogen is present on the α-carbon, thus not susceptible to β-H elimination. This enables APC solutions to exhibit high anodic stability (> 3 V *vs.* Mg); they have become a benchmark RMB electrolyte in which most of the validation and feasibility studies are being carried out,

including in the first part of this study. Despite the electrochemical stability window of the magnesium-metal-anode/APC-electrolyte pair, which extends to 3.3 V, the low overpotential for magnesium deposition, and their moderate 2 mS cm^{-1} ionic conductivity at room temperature, the ability of APC solutions to provide good performance with high-voltage transition-metal-oxide cathodes (such as VO_x materials) is still limited.[25] Attias *et al.*[28] conducted a comprehensive study, comparing most of previously reported electrolyte solutions. In their study, the only electrolyte with CE higher than 99% for Mg deposition dissolution, was found to be DCC (di-chloro complex solutions comprising the reaction products of Bu_2Mg and $EtMgCl_2$ in THF).

Other electrolytes have been proposed as alternatives to APC. One of them is hexamethyldisilazide magnesium chloride (HMDS MgCl), a non-nucleophilic Hauser-base-derived electrolyte, which was reported by Liebenow *et al.*[29] This work constituted a major milestone in electrolyte solutions development, demonstrating the oxidative stability of weak Al–R bonds in an all inorganic salt. Muldoon and coworkers[30] extended the anodic stability of the systems to 3.3 V by adding $AlCl_3$. Adding such a strong Lewis acid induces Lewis acid–base reactions similar to those discussed above and thus changes the composition and structure of the ions in solution, forming more stable solution species, which found particularly wide use in magnesium–sulfur systems.[26,30,31] An electrolyte with a fully inorganic salt that contains chloride species was proposed by Doe *et al.*, who mixed common ethereal solutions of $AlCl_3$ and $MgCl_2$ to prepare solutions of magnesium–aluminum–chloride complexes (MACC).[32] Recently, Canepa *et al.* refined the structural components in this electrolyte solution and their effect on stability, coulombic efficiency, and aging/conditioning.[33] They found that aluminum from the solution is deposited on the magnesium-metal anode in the early cycles, which reduces coulombic efficiency. However, in return, this behavior promotes the stabilization of charged species ($MgCl^+$ and $AlCl_4^-$) dissolved in the electrolyte solutions through a pre-treatment called "conditioning" (repeated Mg deposition/dissolution cycling that cleans the solutions of contaminants) and leads to a smoother plating/stripping of Mg in consecutive cycles.[33] Nevertheless, despite all the conditioning steps and improvements in coulombic and plating/stripping efficiencies, the anode remains unstable above 3.1 V.

Furthermore, fluorinated alkoxide-based electrolytes present solution conductivity of 3.5 mS cm^{-1} and anodic stability of 3.2 V *vs.* Mg^{2+}.[34]

A common denominator among all the electrolyte solutions mentioned above is the existence of corrosive chloride species, which limits not only the electrolyte stability but also the choice of current collectors and cathode active materials.[35,36] Hence, RMB electrolyte solutions have been intensively studied to find chloride-free magnesium salt solutions that exhibit high conductivity and promote fully reversible Mg plating/stripping processes, enabling the use of high-voltage/capacity transition-metal-oxide cathodes.[37–40]

A class of electrolytes based on magnesium borohydride $Mg(BH_4)_2$, the first chloride-free (and halide-free) boron-based electrolyte system, was expected to circumvent this incompatibility between the different components.[41,42] Although this electrolyte was proven to promote reversible Mg plating/stripping, its very poor anodic stability (<1.8 V) is not in line with the energy density requirement of the RMB technology.[41,43] However, this was a steppingstone for the development of non-nucleophilic family of electrolytes.[30,43,44] A key breakthrough was made recently by Fichtner's group, with the successful synthesis of magnesium tetrakis(hexafluoroisopropyloxy)borate $Mg[B(hfip)_4]_2$, which brought new prospects for the cyclability of RMBs and the selection of current collectors and cathode active materials.[38,45] Indeed, this salt may be used with dimethoxy ethane (DME)—an ether-based solvent that has high anodic stability (>4.5 V)—without corrosive Cl component, and electrolytes based on $Mg[B(hfip)_4]_2$ satisfy a variety of requirements for efficient and practical solutions, such as an ionic conductivity ($\sim$11 mS cm^{-1}) more than five folds that of conventional APC electrolyte solutions and excellent long-term cycling stability with low polarization.[11,38,46–49] The uniqueness of this salt originates from its branched carbon structure, which allows the weak coordination of Mg cations, while the presence of proton on the α carbon and the fluorinated β carbon provide oxidative stability (Fig. 2).

As a result, this electrolyte opened up new possibilities to achieve high energy densities through its compatibility with lightweight aluminum current collectors and high-specific-capacity cathode materials, its resistance to side reactions with Mg-metal anodes, and its high anodic stability, suitable for use at high voltage. In addition, the demonstrated stability of this electrolyte toward polysulfide species formed during battery cycling opened the path for research on rechargeable Mg metal–sulfur batteries.[38]

In principle, solid Mg^{2+}-conducting electrolytes can offer a number of advantages over liquid electrolytes. All-solid Mg-ion cells may offer higher level of safety as they do not contain volatile and flammable components and thus, are not prone to leakage and ignition; the ease of manufacturing of cells of all conceivable shapes is also apparent.

To be able to utilize a specific Mg^{2+}-conducting material as solid electrolyte for Mg-ion cells, it should – first and foremost – hold Mg^{2+} ionic conductivity (σ_{ionic}) matching the typical ionic conductivity of liquid Mg^{2+} electrolyte at ambient temperatures. Conductivities of current liquid Mg^{2+}-electrolytes roughly corresponds with Li^+-electrolyte conductivities, and are of the order of a few mS cm^{-1};[50] the best reported Mg^{2+} σ_{ionic} is 11 mS cm^{-1}.[51]

The other requirements are:

- Low electronic conductivity (regarding solid Li^+-electrolyte, a typical ($\sigma_{ionic}/\sigma_{electronic}$) ratio $\sim 2 \times 10^6$).[52]
- Wide electrochemical stability window.
- Satisfactory mechanical properties.
- Being non-corrosive toward common battery components (cell housing, current collectors, *etc.*).
- Non-flammability and thermal stability.
- Mg^{2+} ion transference number close to one.

Currently, most materials, which can satisfy the above requirements, may be divided into three groups:[53–55]

• Metal–organic frameworks – based solid-state electrolytes (MOFs):[56–58]

MOFs present three-dimensional scaffold comprised of metal ions connected by organic ligands; the void space inside the scaffold may be filled with a Mg-salt solution, thus featuring a 3D system of interconnected ionic channels of a few Angstroms in diameter. These emerging Mg^{2+}-electrolytes look promising alternatives to the liquid electrolytes, while the best reported conductivity of such electrolyte is 1.0 mS cm^{-1}.[57]

The study of these electrolytes are at an early stage, though, and the information on Mg^{2+}-transference numbers of MOF-based electrolytes are scarcely available; the best reported Mg^{2+} transference number of the electrolyte of this class is just 0.47.[59] Also, the electrolytes contain some flammable liquid solvents, thus the cells with such electrolytes are expected to be flammable.

• Polymer gel-based solid electrolytes (SGPE) and polymer – solid filler-based electrolytes:[54,60,61]

– The polymer-based gel electrolytes are comprised of polymer matrix (such polymers as PEO, PVA, PVDF, PPO – poly(propylene oxide), PVP – poly(vinyl pyrrolidone)), *etc.* and are usually plasticized by liquid electrolyte with a dissolved Mg^{2+}-salt. This plasticizer/liquid forms an interconnected channels system within a polymer matrix, and Mg^{2+}-ions are transporting along these channels.

– The other type of polymer-based gel electrolyte comprised of SGPE with dispersed nano-sized ceramic fillers, such as SiO_2, TiO_2, ZnO, Al_2O_3, MgO, $MgAl_2O_4$, *etc.*; the composite SGPE – ceramic electrolyte provide enhanced Mg^{2+}-conductivity transference number as compared with pure SGPE.

While the best values of σ_{ionic} for SGPE and filled SGPE are as high as 11 mS cm^{-1},[62] the challenging point is that the transference numbers of these electrolytes are usually low, between 0.66 and 0.26.

Low transference number results in a concentration polarization in the electrolyte, which increases cell overpotential; the problem is aggravated under high current rate conditions. As the matter of fact, there is an inherent trade-off between electrolyte conductivity σ_{ion} and the cation transference number t^+. For instance, Li-ion model cells reaches SOC = 0.75 at 2C current rate and 4.2 V cutoff if σ_{ion} = 4 mS cm^{-1} and t^+ = 1, while in the case of t^+ = 0.4 a SOC = 0.75 may be reached under the same current rate and cutoff voltage only if σ_{ion} = 10 mS cm^{-1}.[63,64]

The other problematic point of the SGPE and filled SGPE is their relatively low mechanical strength and thermal stability, as well as their limited fire safety.

• Ceramic-based solid electrolytes:[16,54]

Much of these materials are purely cationic conductors having transference number t^+ close to one and are non-flammable. Here, we extensively elaborate on this type of materials and its sub-groups.

Hydride-based Mg^{2+}-solid electrolytes ($Mg(BH_4)_2$, $Mg_3(BH_4)_4(NH_2)_2$, *etc.*)[53,65,66]

Hydride-based compounds have hydrogen atoms in the polyanions (such as $[BH_4]^-$), which facilitates the polyanions rotation, thus assisting an effective Mg^{2+} ion transport through the paddle-wheel mechanism. This circumstance gives all the grounds to suggest that this type of materials can have high σ_{ion}. However, so far, the studied materials have ambient temperature conductivity σ_{ion} just around 10^{-5} S cm^{-1}, which is not enough for all-solid Mg^{2+}-ion battery cell applications.

Oxide-based ceramics

The most part of the oxide-based materials exhibits ambient temperature conductivity markedly below σ_{ionic} of liquid Mg^{2+}-electrolyte at ambient temperatures, which is the most problematic aspect of these materials. Up to now, the highest reported σ_{ionic} of this type of material is 0.7 mS cm^{-1} (for MgI_2–$Mg_3(PO_4)_2$ Mg^{2+}-solid electrolyte).[67]

Chalcogenide-based ceramics

In essence, chalcogenide-based Mg^{2+}-solid ceramic electrolytes are in many respects similar to oxide-based Mg^{2+}-conductive ceramics, just having different anionic scaffold, namely S, Se or Te instead of oxygen. Conductivity is the process of Mg^{2+}-ion jumping from one locally-equilibrium position into a similar neighbouring position and the less energy is required for such a jump (*viz.* activation energy E_m), the higher conductivity is. In turn, E_m is inversely proportional to the volume per anion in the case of isostructural scaffolds, so E_m is decreasing in the order $O^- \rightarrow S^- \rightarrow Se^- \rightarrow Te^-$;[68] it is therefore reasonable to expect that chalcogenide ceramic-based Mg^{2+}-electrolytes can have an outstandingly high conductivity.

As a matter of fact, chalcogenide ceramics are very promising Mg^{2+}-solid state electrolytes; the materials have transference number close to one, combining it with high conductivity and advantageous mechanical properties, the materials are safe and fire-resistant, and their manufacturing is relatively simple.[53] Surprisingly, very few electrochemical studies have been reported on chalcogenide –based Mg^{2+}-solid ceramic electrolytes; among these, two MgS–P_2S_5–MgI_2 glass–ceramic systems with low ambient temperature σ_{ionic}[53] and $MgSc_2Se_4$ with a fair Mg^{2+}-conductivity of $\sim$0.1 mS cm^{-1}[69,70] were reported. The problematic aspect was a relatively high electronic conductivity; the ($\sigma_{ionic}/\sigma_{electronic}$) ratio for $MgSc_2Se_4$ was found to be $\sim 2.5 \times 10^3$. The feature was attributed to the inherent property of electronic energy spectra of $MgSc_2Se_4$ crystal structure (the material is a semiconductor with $\sim$2.15 eV bandgap), so was attempted to suppress the electronic conductivity of the ceramic by variation of selenium content (selenium deficient and selenium rich $MgSc_2Se_4$ ceramic), and by aliovalent substitution of scandium with titanium and cerium. The attempts were not successful, though, and it was found that Mg^{2+}-conductivity changes in parallel with electronic conductivity in the case of aliovalent substitutions, namely the decrease of the electronic conductivity accompanies with the essential decrease of ionic conductivity.[70]

The high electronic conductivity clouds the prospects of a practical implementation of chalcogenide ceramic-based Mg^{2+}-solid state electrolytes; this circumstance become a vigorous driving force for in-depth study of the nature of the

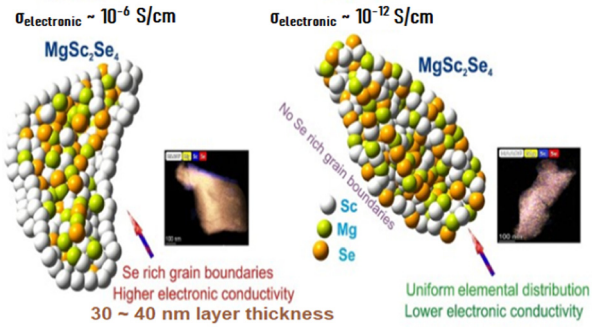

Fig. 3 (left) Model of Se-rich grain boundaries and associated TEM analysis and a model of a uniform distribution of Mg, Se, and Sc and associated TEM analysis (right).

electronic conductivity in ternary spinel chalcogenide $MgSc_2Se_4$ by Kundu *et al.*[8] Mg–Sc–Se ceramics were prepared by high-temperature sintering of the elemental (Mg, Sc, and Se) powder mix, followed by thermal-treatment of the resultant ceramics. It was reported that the morphology of the ceramic strongly depends on the sintering and thermal-treatment modes and a clear correlation between the morphology and electronic conductivity of the ceramic was established.

Particularly, it was found that electron jumping between nano-sized conductive inclusions, which are distributed inside the electronically insulating matrix of $MgSc_2Se_4$, makes the major contribution into the electronic transport in the Mg–Sc–Se ceramic material (the Berthelot mechanism of conductivity). These electronically conductive areas comprise of a mix of metallic-type electronic conductors Sc and ScSe, and the presence and distribution of these inclusions depends on the Mg–Sc–Se ceramic preparation and thermal-treatment modes (see Fig. 3).

The authors of the study were able to eliminate the formation of the above nano-conductive inclusions in the Mg–Sc–Se ceramic matrix by manipulating preparation and thermal-treatment modes of the material, reducing the electronic conductivity by six orders of magnitude; the resulting $MgSc_2Se_4$ ceramic demonstrated low electronic conductivity of $\sim 10^{-12}$ S cm^{-1} without compromising σ_{ionic} of the solid electrolyte having ($\sigma_{ionic}/\sigma_{electronic}$) ratio $\sim 10^8$.

Thus, this work reveals a synthetic method controlling the preparation conditions, eliminating the formation of nano-conductive inclusions, and restricting electronic conductivity of the chalcogenide ceramic – based Mg^{2+}-solid electrolytes, without compromising their high σ_{ionic}.

It should be noted, however, that despite notable progress the development of the chalcogenide-based Mg^{2+}-solid electrolytes are at an early stage, and there is still much of work to be conduct on these materials before they can practically be used in rechargeable Mg-ion cells.

Table 1 provides a summary of the above discussion, describing the state-of-the-art ionic and electronic conductivities of the different solid Mg^{2+}-conducting electrolytes (and related parameters), compared with state-of-the-art liquid Mg^{2+}-conducting electrolyte.

In summary, as mentioned above the $Mg[B(hfip)_4]_2$ electrolyte allows the use of lighter current collector and the development of high energy density cathode materials, which allow reversible two-electron redox with synergetic cationic–anionic contribution in RMB.

3. Anodes

Most RMB studies focus on high-energy cathodes and electrolytes, but anode materials (namely, thin Mg-foil anodes) are also an important factor in achieving high-energy densities.[75–78] A thin foil of pure magnesium metal is naturally the most desired anode, as it may be used as a self-standing anode without the need for an additional current collector.[21,79] The latter feature leads to a significantly higher energy density by avoiding the weight of an additional current collector, which is necessary with Prussian blue analogues, polyanionic compounds, organic compounds, spinel oxides, and insertion-type anode materials in general.[80,81] On the other hand, adverse interactions between a reactive metal like Mg and the electrolyte solution components can rapidly compromise the reversibility of the electrochemical system by promoting the formation of passivating/blocking layers that are not penetrable by the double-charged Mg ions.[11,16,80,82] This limitation related to Mg electrochemistry is at odds with the case of the Li electrochemistry, in which surface films on electrodes (in most cases) behave as solid electrolyte interphases (SEIs), and the singly charged Li ions can easily migrate through surface films comprising ionic Li compounds.[83] To avoid the formation of charge-blocking passivation layers on magnesium, the electrolyte

Table 1 State-of-the-art ionic and electronic conductivities (and related parameters) of different Mg-ion conducting electrolytes

SoA electrolyte system	Transfer Nu.	RT ionic conductivity [mS cm^{-1}]	Electronic conductivity [mS cm^{-1}]	Ref.
Liquids	≥0.5	≥11	NA	51 and 71
Solids				
MOF	≥0.47	≥1.0	N/A	57 and 59
Polymers				
Polymer gel	≥0.73	≥1.0	N/A	54 and 60
Polymer + filler	≥0.66	≥4.8	N/A	54 and 61
Ceramics				
Hydrides	≥0.95	$\geq 1.3 \times 10^{-2}$	$\geq 3 \times 10^{-9}$	65, 72 and 73
Oxides	≥1	≥0.7	Unspecified low values	16, 67 and 74
Chalcogenides	N/A	≥0.1	$\geq 10^{-12}$	8

solution should be based on ether solvents (not reactive to Mg metal) and may contain chloride ions as a desirable component; chloride ions in ethereal solvents seem to interfere with the passivation of Mg anodes and facilitate the transport of Mg ions from heavily solvated states to the electrode surface (Mg deposition on the anode side and Mg intercalation on the cathode side).[25,27,84] For this reason, conventional RMB technology—including the first part of this work—still utilizes the same combination of Mg-metal anodes and chloride-containing ethereal electrolyte solutions as the first publication more than 20 years ago.[17,31,85]

Besides detrimental passivation phenomena, the mechanical properties of Mg metal also cause a limitation to its use.[16,21] In order to ensure their high energy density, magnesium batteries require the use of very thin Mg-metal foil anodes. The preparation of a desirably thin Mg foil anode is very difficult because pure Mg metal is not ductile enough; the hexagonal close-packed (hcp) structure makes it challenging to process Mg metal mechanically below 200 °C.[79] Although the industrial manufacturing of ultra-thin (<100 μm) Mg foils is possible, it is not economically scalable to the level required for battery production.[21,86,87] Thus, the use of pure-Mg metal anodes in batteries should be avoided on the account of their poor mechanical properties. To circumvent this problem, some researchers investigated binary and ternary Mg alloys that have better mechanical properties than pure Mg yet exhibit reasonable electrochemical properties; alloys that have two or more metal species may provide efficient magnesium hosting while offering new properties that the pure Mg metal is unable to provide, including high electronic conductivity, buffering of volumetric changes, and even the advantage of compatibility with different types of electrolyte solutions (*i.e.*, lower reactivity than Mg metal).[79,88]

Theoretically, 3A–5A group metals aluminum (Al), gallium (Ga), indium (In), tin (Sn), bismuth (Bi), lead (Pb) and metalloids silicon (Si), germanium (Ge), and antimony (Sb) can create binary Mg alloys (Mg_xM_y) with high specific capacities at low alloying potentials.[88] However, depending on the electrolyte used and the alloying/dealloying reaction of the candidate, electrochemical activity may be low, which is indeed the case for magnesium alloys with Ge, Si, and Sb. In the case of Mg alloys containing Sn, Pb, or In, some of the problems identified so far are the inevitable side reactions that lead to limited cycle life, the extreme volumetric expansion, and slow kinetics caused by the high Mg^{2+} diffusion barrier, along with possible difficulties in scalability[82,89–93] Alternatively, binary Mg alloys Mg_3Bi_2, Mg_2Si, and Mg_2Ga_5 may be directly used as anode materials without any host.[82,88,94] Bismuth alloys of magnesium metal have attracted some attention owing to their availability, and their reported theoretical volumetric capacity (3783 mA h cm^{-3}), being comparable to that of the Mg-metal anode (3833 mA h cm^{-3}), and their high Mg-cation diffusivity, which make them highly advantageous.[95] However, their theoretical specific gravimetric capacity (385 mA h g^{-1}) is similar to that of the commercial graphite anode (372 mA h g^{-1}) in state-of-the-art Li-ion batteries; therefore, the voltage and low capacity of these RMB systems will render the energy density of the cells too low to be attractive.[88] Moreover, these alloys exhibit extreme volumetric expansion (100–300%), or low electrochemical drive of formation, making them unattractive as anodes in Mg cells. Various strategies (such as nanoscaling, nano-/microstructuring, and film casting), and morphologies(crystalline and amorphous) were employed in the last decade to solve some of these issues, but the challenges remain.[96] As for other alloys, aluminum is the most common addition as a cheap solution to improve the strength of magnesium, as well as to lower the corrosion rate and improve the anode utilization efficiency.[81,97] Other metals, such as zinc (Zn) and gadolinium (Gd), were also reported to improve the workability of pure magnesium metal, although more research is needed for their use in rechargeable magnesium batteries to be considered.[81,86,98]

Multi-element alloys (>2 metals) have been investigated in the search for a promising anode candidate that offers a balance between the electrochemical and mechanical properties, many different binary alloys having failed to behave adequately as self-standing RMB anodes.[88] It is widely thought that adding inactive elements as well as electrochemically active ones might be key to improving electrochemical reversibility and mechanical stability simultaneously.[88] In particular, adjusting the alloy for lower volumetric changes can avoid the cracking and pulverization effects also seen in Li–metal alloys.[42,99] Because magnesium is a widely used metal, a plethora of studies and reports have been published on alloying compounds and their mechanical properties and effects on corrosion.[81] However, a recent computational study focused on cast alloys, which have good processibility and thus scalability, reported that only a few of the studied elements were beneficial for the electrochemical process of plating and stripping.[100] Besides, Yang *et al.* collected several studies which reported the influence of microstructure and composition of Mg alloys on their mechanical properties, ductility, and strength. These kinds of properties might profoundly affect the performance of different alloy anode materials for RMB.[81] Among a wide range of combinations, ternary Mg–Al–Zn alloys are one of the most studied types, owing to their known properties, production methods, refinement, and widespread use in the automotive and aerospace industries.[101,102] The AZ31 alloy (96% Mg, 3% Al, 1% Zn) in the AZ series has attracted special interest because it has a much better ductility than pure magnesium metal. The presence of aluminum and zinc affects the bulk and surface structure, reduces surface reactivity and corrosion.[21,102–104] The better ductility enables to prepare effectively very thin and elastic Mg foil anodes (very important for achieving high energy density). Additionally, AZ Mg alloy anodes were reported to have high utilization efficiency and excellent discharge capacity, increasing the energy density of RMB.[79] These benefits are also due to the total low percentage of dopant (4%) allowing the electrochemical and mechanical properties to be modified while maximizing the amount of active magnesium in the alloy to provide high specific capacities, unlike other AZ series alloys. In other studies, AZ31 alloy itself was doped with small amounts of other elements; however, the change in corrosion

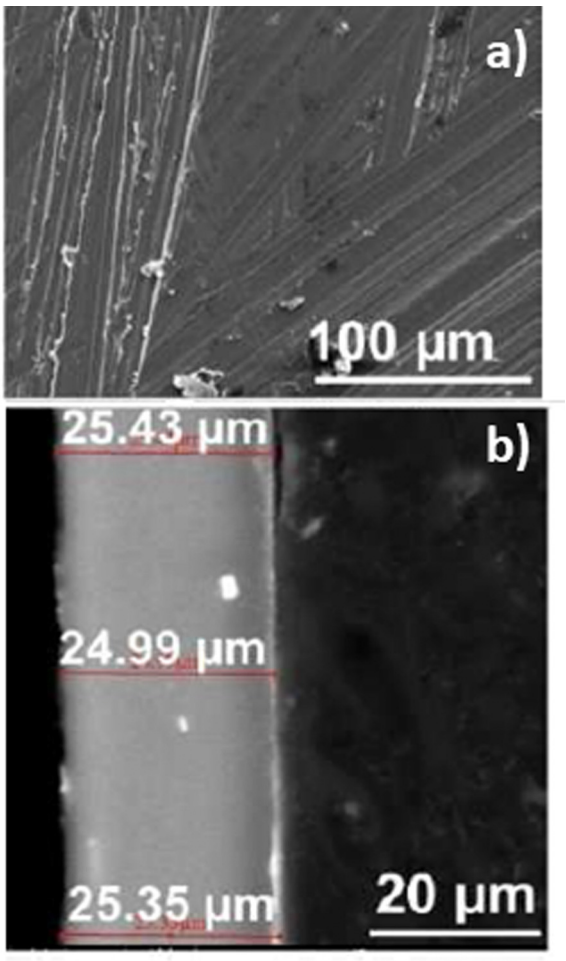

Fig. 4 SEM images of the surface of pristine (a) Mg alloy AZ31 thin film, and (b) cross-section SEM image of ultrathin AZ31 foil.[21]

potential was less than 0.04 V.[97] Recent studies shown the electrochemical and surface chemistry behavior of AZ31 Mg alloy thin foil anodes during Mg dissolution and deposition process is comparable to that of pure Mg foil anodes.[21] Therefore, AZ31 Mg alloy is considered one of the most promising self-standing magnesium-alloy anodes, demonstrating superior electrochemical stability and mechanical processibility for the large production of ultrathin layers, and it is expected to accelerate the maturation of the next-generation high energy density RMB technology.[21] It is important to note that the electrochemical behavior of thin foil electrodes made of AZ31 Mg alloy, is expected to be very similar to that of pure Mg foils (thus ensuring an optimal energy density for the resulting Mg batteries). The combination of performance and processability makes AZ31 Mg alloy the anode material of choice for Mg battery cells (Fig. 4).

4. Cathodes

The conventional state-of-the-art RMB, which was developed two decades ago, uses a CP Mo_6S_8 cathode prepared through the high-temperature synthesis of $CuMo_3S_4$ followed by the electrochemical removal or chemical leaching of copper.[17] The CP contains three-dimensional channels facilitating Mg^{2+} transport and a unique metallic electronic structure providing easy accommodation of electrons.[105,106] The charge of the magnesium cations is balanced by sulfur atoms in the structure, with a screening cloud that enables weak electrostatic interactions and 2+ charge shielding, leading to a low migration barrier (570 meV) and fast diffusion (10^{-12} cm^2 s^{-1}) at room temperature in comparison with other materials.[75,76] However, its low average working voltage of 1.1 V (an upper intercalation voltage range at 1.3–1.1 V into the CP ''inner ring'', and an intercalation plateau at around 1.05 V into its ''outer ring'' accommodation sites) in combination with its low theoretical (129 mA h g^{-1}) and practical capacity (approximately 70–80 mA h g^{-1} *vs.* Mg/Mg^{2+}, ~112 mA h g^{-1} *vs.* Li/Li^+, measured in a coin cell configuration) makes it a non-competitive cathode.[17,107–109] Consequently, in this study, a CP cathode is only utilized to establish an electrochemical performance reference of the current conventional RMB technology; for a cell to reach the desired high energy density, the CP cathode should be replaced with a high working-voltage/capacity alternative.

Among all the cathode materials proposed, only a few groups of candidates demonstrate adequate properties (Fig. 5), and further study is needed to find a suitable cathode for practical RMB.[110,111] So far, transition metal oxides and sulfides (TMOs and TMSs), layered transition metal chalcogenides (TMCs), layered and spinel oxides, Prussian blue analogues (PBAs), vanadates, silicates, polyanionic phosphates, and even organic compounds have been studied as potential secondary magnesium battery cathodes.[11,12,15,16,24,25,43,112–118] TMOs (*i.e.*, Co_3O_4, Mn_2O_3, Mn_3O_4, *etc.*) constitute one of the most studied groups in state-of-the-art Li-ion batteries on account of the high capacities they can provide due to the crystal lattices which contains tunnels and pathways for intercalation.[119] In RMBs, according to early studies, TMOs can generate relatively high capacity and working voltages,

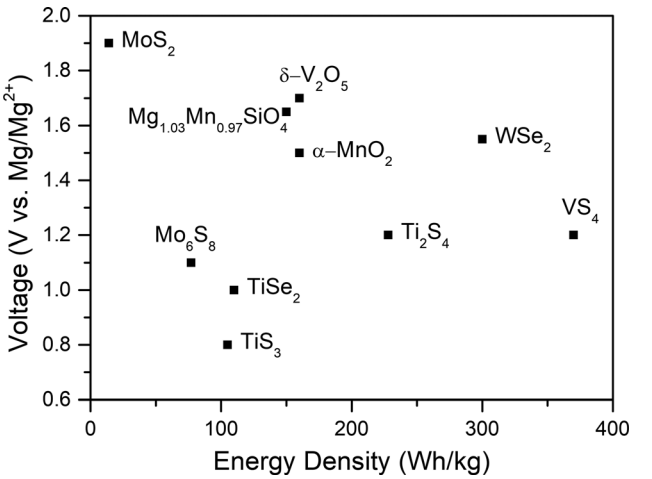

Fig. 5 Voltage (*vs.* Mg/Mg^{2+}) and energy density (calculated based on the cathode parameters only) of several cathode materials that may be relevant to RMBs.[111]

although reversibility is hampered by the interaction of the double charge of magnesium with the crystal lattice.[120,121] Moreover, while conventional APC solutions—containing chlorides—present compatibility problems with these materials, new high-stability boron-based electrolytes might spark a new research avenue for the use of TMOs in RMB.[24,105]

On the other hand, chalcogenides have better properties, thanks to S^{2-} and Se^{2-} having a larger ionic size than O^{2-}, thus providing wider channels.[122] Additionally, the weak coulombic interactions in the sulfur layers of their structure ease the ionic mobility of doubly charged magnesium ions and the Mg^{2+} desolvation in electrode/electrolyte interfaces.[50,75] For cathodes such as TiS_2, TiS_3, or Ti_2S_4, the working voltages are in fact lower than in CP cathodes, although the theoretical capacities and energy densities they can provide are slightly higher.[76] Another molybdenum chalcogenide alternative to Mo_6S_8 is MoS_2. It has a higher working voltage (1.9 V) than most cathodes and has a theoretical capacity of 223 mA h g^{-1}. However, its cyclability is inferior to that of CP.[77]

Promising studies have explored selenides, such as WSe_2, which can provide high working voltages (1.5 V) and high specific discharge capacities (203 mA h g^{-1}).[106] However, this material loses ~20% of its initial capacity after a mere 50 cycles. Therefore, despite their many advantages, the cyclability of chalcogenides needs to be improved for them to be used in practical RMBs.[43,123]

PBAs, with a formula of $A_xM_A[M_B(CN)_6]\cdot zH_2O$ (A is an alkali metal, M_A and M_B are transition metals), are the subject of a vast body of literature, in particular studying the intercalation of different valency cations and of some small molecule solvents in their open framework with 3D diffusion channels.[40,43,124] The reason for the successful insertion of a wide variety of cations into PBAs lies in the coordination of triple-bonded cyanide groups (CN^-) with the metal ions and the opening of the structure caused by the increase in the separation between transition metal ions (Ni, Cu, Fe, *etc.*).[43,125] Nickel hexacyanoferrate (NiHCF) has been shown to intercalate Mg^{2+} ions successfully, although at low capacities and in the presence of a cell with flooded electrolyte. Moreover, the structural crystal water in PBAs and the capacity contribution originating from the inserted electrolyte solvent molecules prevent a full understanding of the working mechanism of these cathodes.[10,125]

Among the many different cathode materials used for intercalation, polyanionic compounds are some of the most studied.[40,78] These compounds are mostly sought after because of their stable 3D network structure, high voltage, and weak electrostatic interaction with the mobile cation, a set of properties that, in principle, make them good RMB cathode candidates.[78,126] In particular, olivine-type silicates ($MgMSiO_4$, M = Fe, Mn, Co) can intercalate magnesium at a high working voltage and capacity ($Mg_{1.03}Mn_{0.97}SiO_4$: ~1.6 V *vs.* Mg/Mg^{2+}, ~210 mA h g^{-1}) and have a structural ability to ease volumetric expansion.[106] NASICON-structured phosphates (NASICON = Na super ionic conductor), such as $Mg_{0.5}Ti_2(PO_4)_3$ and $MgZr_4(PO_4)_6$, were also studied.[122] The first composition, $Mg_{0.5}Ti_2(PO_4)_3$, was only studied for its magnesium intercalation, and though it has Mg in its structure, it is probable that it cannot be used in a full magnesium battery because of the initial oxidation state of titanium (Ti^{4+}).[122] As for $MgZr_4(PO_4)_6$, it is only promising at high temperatures (~800 °C), where its ionic conductivity is high (6.9×10^{-3} S cm^{-1}) because of the formation of a secondary phase that decreases the grain boundary resistance.[122]

Vanadium and vanadates provide an important advantage due to their flexible oxidation states, keeping local electroneutrality and lowering the Mg^{2+} diffusion barriers.[76,122] V_2O_5, VS_2, and VS_4 are among many compositions that have been studied for RMB.[76,115,122] One of the motivations for the extensive study of V_2O_5 polymorphs is their theoretical energy density of 660 W h kg^{-1}, which depends on the V^{5+}/V^{3+} redox couple.[122] Specifically, α-V_2O_5 was reported to reversibly intercalate magnesium into its structure with a specific capacity of 280 mA h g^{-1}.[127] A recent computational study was carried out to clarify the intercalation mechanism of Mg^{2+} in α-V_2O_5 under equilibrium conditions; it concluded that the intercalation through the formation of δ-$Mg_xV_2O_5$ ($0 < x < 1$) is hindered kinetically, while a metastable insertion path of Mg in α-V_2O_5, leads to an ε-$Mg_{0.5}V_2O_5$ phase, that is more consistent with experimental data.[128,129] Other studies have confirmed that the phase transformation rearranges the *a*-axis layer stacking, changing the cation coordination for intercalation sites.[129] Moreover, the Mg^{2+} migration is calculated to be faster and energetically more favorable in the δ phase, so methods for the solid-state synthesis of δ-MgV_2O_5 and its electrochemical demagnesiation have been seen as a way to enhance the sluggish kinetics and low performance of V_2O_5.[128]

As one of the most promising cathode materials, VS_4 has attracted a lot of attention for its one-dimensional chain-like crystal structure along the *c*-axis composed of V^{4+} and sulfur dimers (S_2^{2-}) bound by weak van der Waals forces.[130,131] The weak forces of interaction within the material and the repeating chain distance (5.83 Å, (110) plane for monoclinic VS_4), which is much larger than the diameter of Mg^{2+} cations (1.44 Å), allow easy Mg-ion transportation through the open channels and support good electrochemical performance.[75,111,132,133] Additionally, the VS_4 structure was previously reported to present a Peierl distortion (dimerizations) due to its one-dimensional chain structure; in such structures, a perfect crystal is electronically unstable and goes through a natural lattice periodicity reordering to allow the electrons to sit at lower energy.[115] This lattice distortion also introduces new bandgaps with a smaller energy difference (~1.0 eV in case of VS_4) that provides high electronic conductivity.[132,134] In terms of electrochemistry, VS_4 has been shown to exhibit an initial capacity of 250 mA h g^{-1} at C/12, while a VS_4/rGO composite has shown an extraordinarily high specific capacity of approximately 330 mA h g^{-1} at a 100 mA g^{-1} current density, with an initial specific capacity of 408 mA h g^{-1}.[111,115] Besides, in another recent study, VS_4 nanodendrites have demonstrated a specific capacity of 74 mA h g^{-1} at a high current density of 500 mA g^{-1} after 800 cycles.[75] Overall, these results show promising rate capability and cyclability, and most importantly, a near 5-fold improvement in practical energy density in VS_4 cells in

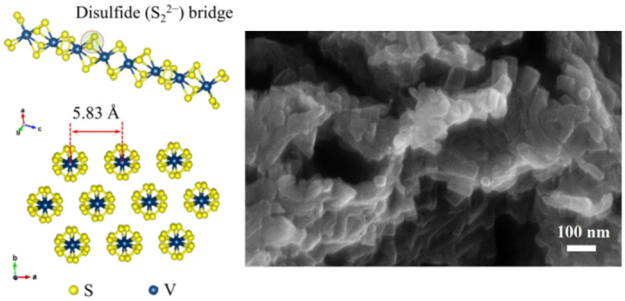

Fig. 6 Molecular structure of material VS4/rGO and SEM image with a higher magnification.[111]

comparison to CP cells. Indeed, the minimum acceptable specific capacity and working voltage established by Gregory *et al.* is 230 mA h g^{-1} at 1.5 V, corresponding to a specific capacity of ~315 mA h g^{-1} at 1.1 V, which is very similar to the experimental results with VS_4.[24,105,111]

As stated previously, VS_4 (Fig. 6) presents competent electrochemical performance, such as its high specific capacity and is a model material for reversible two-electron redox reaction with synergetic cationic–anionic contribution. Therefore, in this study, VS_4 was chosen as the most promising cathode material for competitive advanced RMB pouch cell prototypes to be used in commercial storage applications in the near future.

5. Experimental section

High-purity Mg metal foil (99.9%, 100 μm) was provided by Gelon LIB group and Chevrel Phase (CP) Mo_6S_8 by the American NEI Corp. (1 kg). Pouch cell cathodes were processed in a pilot plant line using CP/carbon black (C45)/PVDF (90 : 5 : 5) at an 11.8 mg_{CP} cm^{-2} loading (1.6 mA h cm^{-2}) on both sides of a nickel current collector (Gelon LIB group, 20 μm), while coin cell cathodes on nickel current collectors were produced in our laboratory by the doctor blade technique at a 3.5 mg_{CP} cm^{-2} loading.

Pouch cell prototypes consisted of five pure-magnesium metal-foil anodes (44 × 61 mm) and four double-sided cathodes (43 × 60 mm) stacked with a double-layer polyolefin-based separator in between, unless indicated otherwise.

The 2025-type coin cells consisted of one layer of a magnesium metal foil anode, a single-side coated cathode, and a layer of Whatman glass fiber (GF/F) in between the electrodes. The assembly of coin cells was done in a high-purity (99.999%) Ar-filled glovebox (MBraun, Germany) under ideal conditions (O_2 < 1 ppm, H_2O < 1 ppm), whereas pouch cells were assembled in a dry room (dew point −50 °C) using standard pouch cell packaging foil (Targray) and nickel tabs (Gelon LIB group). The assembly technique of the scaled-up conventional RMB pouch cells was the same used for conventional lithium-ion batteries.

The pouch cells were sealed under vacuum conditions in the above-mentioned glovebox. APC electrolyte solutions were prepared following procedures described elsewhere.[17,38] The amounts of electrolyte solution used were 100 μL in each coin cell and 3 mL in each pouch cell. Prior to each cycle life test,10 activation cycles were applied.

The calculation spreadsheets for the energy density and mass distribution values given in Table 2 of the article are in the ESI.†

6. Design and properties

Materials research experiments for energy storage applications are habitually performed in a coin cell setup, an economical small-scale configuration that necessitates only small amounts of active material and is adapted to the materials discovery, characterization, and performance-testing stage. However, the testing parameters and results thus obtained do not always accurately reflect the working parameters of practical cells, and the cells may show differences in the ratio of active materials in the electrode formulation and in active material loading, positive/negative electrode balancing, efficient components selection, electrolyte amount, and other aspects of an industrial battery design.

In this section, the differences between coin cells and pouch cells are highlighted, and further impacts of the pouch cell modifications with novel materials on energy density, mass distribution, and battery design are estimated.

6.1. Conventional RMB based on a CP cathode/standard APC electrolyte solution/pure Mg metal anode

6.1.1. Coin cells. Coin cells built with hard upper and bottom shell cases prevent volumetric changes; spacers create a reliable physical support against bending for the electrodes, and a spring ensures a good contact of all the components with each other, which provides an ideal environment for the electrochemical characterization of the materials. Additionally, other cell components are used that are particularly unrealistic in terms of industrial applications. Glass fiber (GF) separators are thick (250 μm) and highly porous and thus need significantly more electrolyte solution than polyolefin (PO) separators to be fully wetted—and the electrodes can be wetted only when the separator is completely wet. Therefore, the use of GF leads to an excessive amount of electrolyte, or "flooding", which also changes the kinetics within the coin cells as the abundance of some species affects magnesium plating/stripping.[135] Furthermore, the properties of GF are very different from those of thin, PO-based separators used in state-of-the-art batteries.[136] Because of their relatively poor surface affinity and low porosity, PO-based separators hold less electrolyte and allow a higher proportion of the electrolyte to be used by the electrodes. On the other hand, the wettability of GF, resulting from its hydrophilic SiO_2 surface and air permeability (Gurley number of 2.2–19 s/100 mL in^{-2}), also varies greatly in comparison with that of PO-based separators (200–800 s/100 mL in^{-2}).[136] Thus, the use of GF separators makes it difficult to assess the industrial relevance of some active materials and electrolytes, especially where the size of the shuttling species is large (Table 2).

Table 2 Summary of cell components, properties, and energy densities in conventional RMB coin cells, modified pouch cells (first generation), and higher generation RMBs in pouch cell configurations (green: experimental values, blue: estimated values)

Coin Cell	Pouch Cell			
Conventional RMB	**1st Generation Conventional RMB**	**2nd Generation Al CC + Borate Electrolyte**	**3rd Generation Al CC+ VS_4+ Opt. Electrolyte**	**4th Generation Al + VS_4 + AZ31 +Electrolyte**
Pure Mg Foil (100 μm) 214-fold excess	Pure Mg Foil (100 μm) 33-fold excess	Pure Mg Foil (100 μm) 33-fold excess	Pure Mg Foil (25 μm) 7-fold excess	AZ31 Alloy (25 μm) 1.7-fold excess
Nickel (20 μm)	Nickel (20 μm)	Aluminium (12 μm)	Aluminium (12 μm)	Aluminium (12 μm)
CP (3.5 mg/cm²) single side	CP (11.8 mg/cm²) double side	CP (11.8 mg/cm²) double side	VS_4 (11.8 mg/cm²) double side	VS_4 (11.8 mg/cm²) double side
Glass Fiber (250 μm, 1 layer)	PO-based (50 μm, 2 layers)	PO-based (50 μm, 2 layers)	PO-based (50 μm, 2 layers)	PO-based (25 μm, 1 layer)
APC $AlCl_3$/PhMgCl in THF (220 μL/mAh)	APC $AlCl_3$/PhMgCl in THF (19 μL/mAh)	Borate-based $Mg[B(hfip)_4]_2$ in DME (19 μL/mAh)	Borate-based $Mg[B(hfip)_4]_2$ in DME (2.65 μL/mAh)	Borate-based $Mg[B(hfip)_4]_2$ in DME (2.65 μL/mAh)
2 Wh/kg_{cell}	**18 Wh/kg_{cell}**	**20 Wh/kg_{cell}**	**118 Wh/kg_{cell}**	**157 Wh/kg_{cell}**
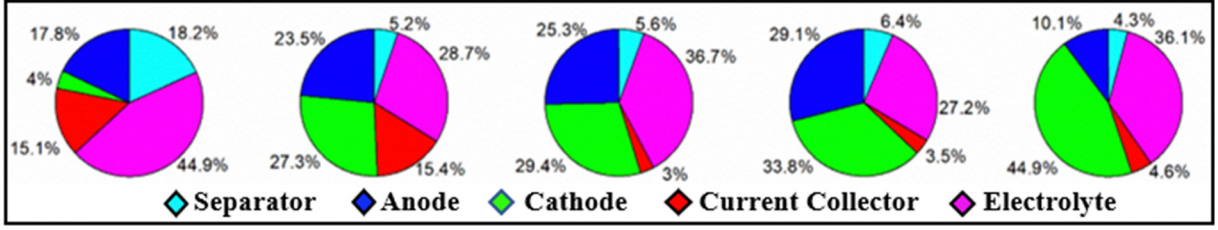				

This affects the battery in two ways, impacting both the electrolyte–volume/capacity ratio and anode/cathode balancing, causing disproportionality.[136] Coin cells use cathodes with a low loading of active material (3.5 mg_{CP} cm^{-2}) coated on a single side of the current collector. The electrolyte–volume/capacity ratio is already affected by the excessive amount of electrolyte solution made necessary by the GF separator, and the low loading of active material and limited area coverage aggravate it. In this work, the electrolyte–volume/capacity ratio for the coin cells was 214 μL mA^{-1} h^{-1} (see calculations in the ESI†), more than 100 fold that used in industrial Li-ion batteries (2–4 μL mA^{-1} h^{-1}).[137,138] Additionally, the structural parts of a coin cell, such as the spacers and springs that hold the battery active materials in place and in continuous contact, create a so-called ''dead volume'', which adds to that in the pores of a GF separator.[139] Although dead volume also exists at the edges of pouch cells, it can be resolved by increasing the number of layers in the pouch cell to decrease the ratio between the dead volume and the volume of active components.[139] In the coin-cell configuration, anode/cathode balancing is also impaired by the excessive use of magnesium metal, the anode having a typical thickness of 100 μm. Consequently, the anode/cathode capacity ratio is dramatically unbalanced, going up to 214-fold without the benefit of increased performance, whereas in industrial Li-ion batteries, the capacity of the anode is approximately 10% higher than that of the cathode to account for the losses due to the formation of surface films during the first charging process of the cell.[139–141]

The cathode current collector accounts for a large portion of the final weight of the battery. It is well established in the literature that aluminum current collectors are a standard for high-voltage cathodes in Li-ion batteries because of their lightness ($density_{Al}$ = 2.7 g cm^{-3}) and the already established methods to produce thin foils (12 μm).[142] The compatibility between the electrolyte solution and the current collector is also essential for the reversibility and good cycle life of rechargeable batteries.[39]

As mentioned earlier, aluminum cannot be utilized in conventional RMBs because of corrosive chloride species in APC electrolyte solutions; thus, nickel current collectors are used for

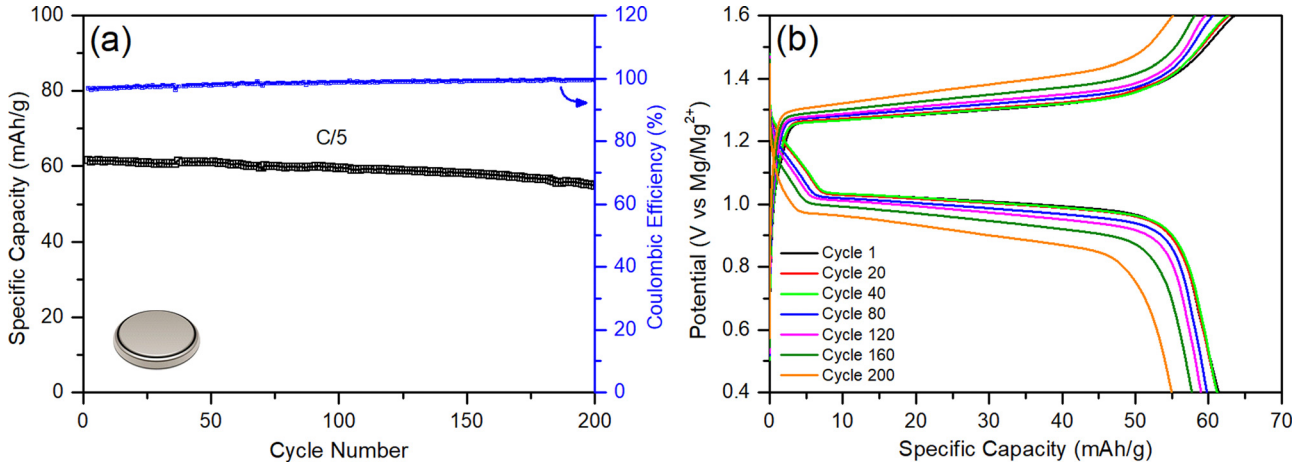

Fig. 7 Conventional RMB-chemistry coin cell: (a) galvanostatic cycling performance at C/5, and (b) voltage profile.

electrochemical stability reasons, although they are thicker and intrinsically heavier (20 μm, density$_{Ni}$ = 8.9 g cm^{-3}).[26]

When all these components, their properties, and amounts are factored in, they cumulatively generate very poorly optimized coin cells with flooded electrolyte solutions, poor anode/cathode balancing, and weight inefficiencies, leading to a poor energy density (2 W h kg^{-1}); this is despite the fact that RMBs assembled in coin cells show comparable specific capacities to those reported in the literature (60 mA h g_{CP}^{-1}) and can be cycled more than 200 times with coulombic efficiencies above 96% (Fig. 7). The mass distributions of above-mentioned coin cells are given in Table 2 (see Experimental details in the ESI†). Accordingly, almost half of the battery mass (44.9%) comes from the flooded APC electrolyte used to wet the thick GF separator (18.2%). In parallel, the excessively thick magnesium-metal anode represents 17.8% of the total mass of the battery prototype in the coin cell configuration. The low loading of CP active material on the cathodes only contributes 4% of the total mass of the battery, and the thick nickel current collector corresponds to 15.1% of the battery mass. Even when the contributions of the binder and the carbon additive is included, the electrochemically inactive nickel current collector component makes up a disproportionate 79% percent of the total cathode weight.

Clearly, all these issues must be addressed for practical RMB pouch cells design to be achieved for the first time.

6.1.2. First RMB pouch cell prototypes. Building the first conventional-chemistry pouch cell RMB prototypes primarily involved the replacement of the laboratory-scale components with others that are more industrially relevant to address the inefficiencies of the typical Mg-ion coin cell design (Table 2).

The GF separator in the coin cell configuration was replaced with a double layer of a thin PO-based separator; this decreased the associated mass percentage from 18.2% to 5.2%, thanks to the great difference between the unit weights of the GF (17 mg cm^{-2}) and PO separator (single layer, 3 mg cm^{-2}). This change also allows the amount of APC electrolyte used in the cells to be decreased dramatically, from 44.9% to 28.7% of the total mass.

The format was changed from a single-sided coating with a low loading of material (3.5 mg_{CP} cm^{-2}) to a double-sided coating with a high loading of material (11.8 mg_{CP} cm^{-2}); this translated into a change in electrolyte–volume/capacity ratio from 214 μL mA^{-1} h^{-1} in the coin cell setup to 19 μL mA^{-1} h^{-1} in the pouch cell setup. Additionally, the increase in active material loading and the doubling of surface coverage by the active material had a direct impact on the current collector/total-cathode mass ratio, which improved from 79% to 36%. Another ratio pointing to an optimized configuration of the components is the anode/cathode capacity ratio, which must be balanced to get the best performance out of the used materials: this ratio was improved from a 214-fold excess of anode active material (Mg) to a 33-fold excess, even though the anode/cathode layer ratio was changed from 1/1 in coin cells to 5/4 in pouch cells. Overall, the combined mass of the electrolyte solution and the electrochemically inactive separator was decreased, and the relative amount of cathode active material was dramatically increased. As shown in Table 2, the optimization of these three components in relation to each other has the most drastic effect on the mass distribution.

The first pouch cell RMB prototypes were prepared by implementing only these design changes and their electrochemical performance was characterized by galvanostatic cycling at C/10. The cells demonstrate an energy density of 18 W h kg^{-1} (a 9-fold improvement) and a 100% energy-density retention even after 200 cycles (Table 2 and Fig. 8(a)). The coulombic efficiencies of the cells were initially >97% and improved to 99% during cycling. The voltage profiles in Fig. 8(b) present excellent reversibility and show kinetics that are characteristic of a Mg^{2+} intercalation reaction into the "inner ring" and "outer ring" accommodation sites of the CP cathode structure.[7,108] Although the charging curves show a small overpotential (0.1 V) for the plating reaction and end with a slope for Mg^{2+} deintercalation, the results obtained with these pouch cells are in very good agreement with the results presented

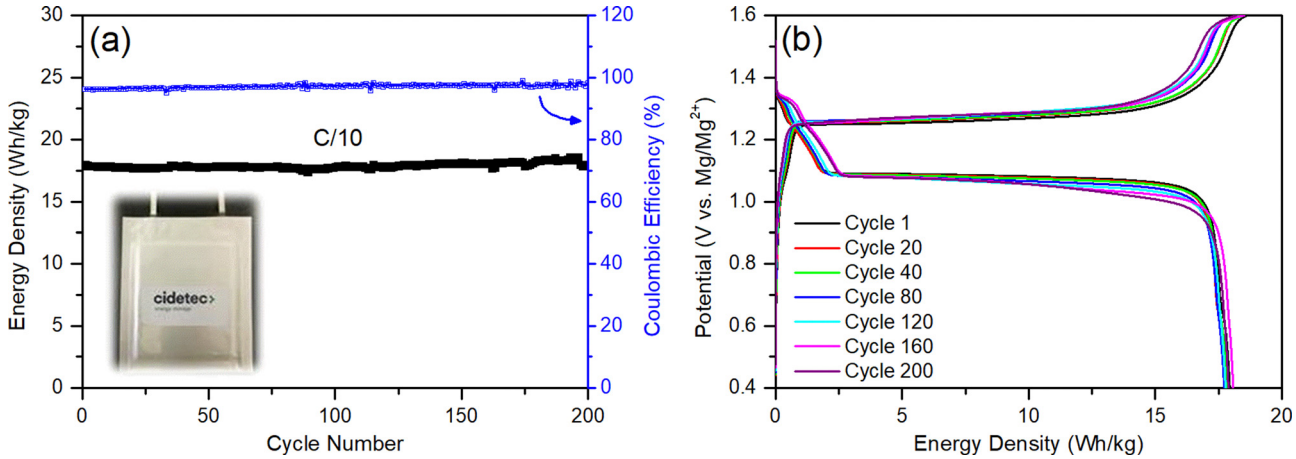

Fig. 8 (a) Energy density and coulombic efficiency of the first generation conventional RMB pouch cell over 200 cycles. (b) Voltage profiles at C/10 for cycles 1, 20, 40, 80, 120, 160, and 200.

above for the coin cells and are in line with the kinetics data described in the literature.[143,144] Besides, no relevant changes in the temperature of the cells were detected by external thermocouples that were attached to them. This 9-fold improvement in energy density can be considered a great achievement, especially in the first pouch cell prototypes ever presented in the literature; nonetheless, these cells are far from meeting accepted industry standard, and the cells' design need further optimization to reach a cheap, environmentally friendly and well-performing battery system that can penetrate the energy storage markets.

6.2. Impact analysis of advanced materials on RMB performance and the total mass distribution in the cells

Pure-magnesium metal-foil anodes, standard APC electrolyte solutions, and CP cathodes on nickel-foil current collectors were utilized to establish the conventional RMB technology (which can be considered the most reasonable benchmark) as a reference to evaluate the electrochemical performance and mass distribution in the prototype cells. However, even after a considerable optimization of the cell design, it is clear that the battery components have their limitations, which restrict the cell performance from reaching a level suitable for practical applications. Therefore, a higher energy density in such cells requires the replacement of the conventional RMB technology components presented above and the adoption of advanced RMB chemistries.

After collecting solid data related to first generation RMB prototypes in practical pouch cells configuration, loaded with most appropriate reference materials, demonstrating stable cycling performance we move to the second stage of this work and related paper. Based on solid data that we have, related to alternative components that can take the RMB technology further and upgrade it considerably in terms of energy density, we can estimate the performance of much more advanced models of RMB, in similar pouch cells (same configuration as described in Section 6.1). We show below how the possible use of new and novel components improves the energy density of RMB technology, thus making it more practically important.

A solution comprising the $Mg[B(hfip)_4]_2$ salt in DME, a thin AZ31 magnesium alloy foil anode, and a VS_4 cathode were chosen for the final step in order to design more advanced RMB prototypes (in pouch cells similar to that described above). The components chosen for the next step are expected to have a less corrosive nature, higher stability, better self-standing properties, easier mechanical processibility, higher practical capacity, and improved cyclability.

To evaluate the impact of these changes, the cell components, mass distributions, and resulting performance were discussed in detail: the step-by-step replacement of each component was considered and the effect on the cell parameters and performance were estimated. In order to ensure that the methodology used in the simulation of the energy density of the different versions of magnesium batteries made, it has been decided to use this tool with a reference battery system based on LFP/graphite (Table S6, ESI†). The energy density values obtained for this base line system (135 W h kg^{-1}) agrees with the values reported in the state of the art.[145,146]

6.2.1. Estimated effect of the borate electrolyte and selection of alternative current collectors. The energy density and manufacturability of the first conventional RMB pouch cells should be improved by replacing the heavy nickel current collector, thus decreasing the overall battery weight; the use of a chloride-free electrolyte solution based on the $Mg[B(hfip)_4]_2$ salt in DME resolves the compatibility issue with the much lighter aluminum current collector.[147] This new solution was also proven to be fully compatible with the benchmark CP cathodes (despite the absence of chloride moieties).[144] Hence, it is theoretically possible to build cells with a CP cathode on an aluminum current collector, a new borate-based electrolyte solution, a double-layered PO separator, and a pure or alloyed magnesium-foil anode.

In such a case, the estimations show a net 82% decrease in the mass of current collector, on account of the large difference between the densities of aluminum and nickel and the possibility of producing thin aluminum foils. Although the replacement of the electrolyte solution leads to an increase in mass because the new borate-based electrolyte solution (3 mL in the

pouch cells) has a higher density (by 18%) than the APC benchmark solution; the mass of the average pouch cell sees an overall decrease of 7% from the combined changes of the solution and the cathode current collector. As a result of the estimated changes in mass, the calculated mass distribution of the main components of the cell is *ca.* 29.4%, 25.3%, 5.6%, 36.7%, and 3% for the cathode, anode, separator, electrolyte solution, and Al current collector, respectively, as presented in Table 2.

Compared to the first-generation RMB pouch cells, the current-collector/total-cathode mass ratio (36%) is 9.3% lower in the second-generation pouch cells, indicating an improvement in weight efficiency through a decrease in the mass of the inactive components.

Overall, the above-described changes implemented in the second-generation RMB pouch cells (using the same CP cathode material) should lead to an energy density of 20 W h kg^{-1}, a 7% enhancement over that of the first-generation cells.

6.2.2. Estimated effect of the VS_4 cathode and optimized amount of electrolyte solution. As mentioned earlier, a practical capacity of 330 mA h g^{-1} at 100 mA g^{-1} was confirmed for VS_4/rGO, with an initial specific capacity >400 mA h g^{-1}.[111] Even in the case of a conservative assumption of a specific capacity of 300 mA h g^{-1}, incorporating a VS_4/rGO cathode in the above-described pouch cell, using the same mass and loading (11.8 mg_{VS4} cm^{-2}), should increase its capacity and energy density by more than 5 times compared to the second-generation cell containing a CP cathode.

Other implications of increasing the cathode capacity are an improvement of the anode/cathode capacity balancing and solution–volume/capacity ratio. The previous 33-fold excess of pure-magnesium metal-anode capacity decreases to 7-fold when VS_4/rGO is used, indicating a more efficient use of the cell weight. In addition, the amount of electrolyte solution (3 mL, 19 μL mA^{-1} h^{-1} *vs.* CP capacity) was decreased to 1.935 mL, converging to the amount seen in industrial Li-ion batteries (2.65 μL mA^{-1} h^{-1} *vs.* VS_4 capacity). While the optimization of the amount of electrolyte solution was estimated to decrease the net cell weight by 13%, compounding it with an improvement in capacity by the change of cathode resulted in a calculated pouch cell energy density of 118 W h kg^{-1} (Table 2), in what can be termed as the third-generation cell in the framework of the systematic studies described herein.

6.2.3. Estimated effect of AZ31 magnesium alloy foil anodes. As the final step, leading to our 4th generation RMB pouch cell prototype, we evaluated replacing the pure Mg foil (100 μm) anode with a thin AZ31 foil. This substitution was very important, because the use of the much more ductile AZ31 anode material enables the preparation of 25 μm thin self-standing foils (a 4-fold reduction in thickness compared to the previous stages based on pure Mg foil anodes).

The substitution of the anode component should reduce the Mg excess with respect to the cathode capacity to a more realistic 69%. Further reduction of excess magnesium may be achieved by decreasing the thickness of the alloy (only a 35% anode capacity excess should be seen when using 20 μm thick Mg anodes). To further diminish the mass percentage of the inactive components, the two layers of PO-based separator (50 μm) between each stack may be reduced to one (25 μm). In this sense, Table 2 contains the estimated energy density of our 4th generation RMB pouch cell prototype, whose calculations are explained in detail in the ESI.† Consequently, the calculations show the following estimated mass distribution for the final, 4th generation RMB prototypes (in pouch cells): *ca.* 44.9%, 10.1%, 4.3%, 36.1%, and 4.6% for the VS_4 cathode, AZ31 alloy anode, PO-based separator, borate-based electrolyte solution, and aluminum foil current collector, respectively (Table 2).

The overall impact of the changes carried out between the first conventional RMB pouch cells and the estimated advanced chemistry in the 4th generation RMB pouch cells is emphasized in Table 3. The total weight is lowered by 40%, mainly thanks to the substitution of the current collector, the optimization of the electrolyte, and the reduction in anode thickness. In addition, the excess magnesium with respect to cathode capacity is reduced significantly (95%) by changing the cathode active material, the anode type and its thickness. The electrolyte–solution–volume/capacity ratio is also decreased by 86% by reducing the amount of electrolyte in the cells down to industrial battery levels and by using an active material that has a high specific capacity at the cathode side. The substitution of the heavy nickel current collector with an aluminum current collector reduced the current-collector/total-cathode mass ratio by 74%. Hence, by implementing all these changes, the practical energy density of the 4th generation RMB pouch cells (without taking into account the case) should reach values of approximately 157 W h kg^{-1}, an 855% enhancement compared to the first-generation pouch cell of this work.

Importantly, these calculations are based on the conservative capacity values reported for VS_4 cells.[111] If coin cell capacity values can be realized in pouch cells, as was the case for assembled CP/APC/Mg pouch cell prototypes, the resulting energy density of next-generation RMB could thus reach impressively high values. Alternatively, if a cathode material with a higher working voltage than VS_4 (ideally >2.0 V) can be used, advanced RMB would easily become more commercially relevant and even be able to compete with other post-lithium battery technologies, such as Na-ion batteries, in the field of stationary storage technologies. This is now made plausible (yet calls for experimental validation) by the use of high

Table 3 Comparison of various parameters between a conventional RMB pouch cell and a conservatively estimated advanced-chemistry 4th generation RMB pouch cell

	Conventional RMB (1st gen)	Adv. RMB (4th gen)	Impact (%)
Weight (g)	10	6	−40
Excess Mg *vs.* cathode capacity	30-fold	1.7-fold	−95
Electrolyte/capacity ratio (μL mA^{-1} h^{-1})	18	3	−86
Current coll./total cathode mass	35%	9%	−74
Energy density (W h kg^{-1})	18	157	+855

capacity/voltage TMO cathodes in the presence of the new Mg borate-based electrolyte solutions, which avoids the use of chloride moieties present in previously used solutions.

7. Conclusions

In summary, we have demonstrated a conventional-chemistry pouch-cell RMB prototypes for the first time, using a Mg-metal anode, a CP cathode, and an APC electrolyte solution. To overcome the electrochemical limitations of these materials, we proposed a step-by-step strategy to replace the components with a laboratory-validated aluminum current collector, a $Mg[B(hfip)_4]_2$/DME electrolyte solution, a VS_4 cathode, and a very thin AZ31 magnesium alloy anode to reach a competitive, high-energy density, advanced RMB chemistry.

The RMB prototypes based on the conventional chemistry was used as a reference to compare the total mass, mass distribution ratio and electrochemical performance when estimating the impact of systematic changes of components. The battery design factors such as excess magnesium with respect to the cathode capacity, the electrolyte–volume/capacity ratio, the current-collector/total-cathode mass ratio and the mass distribution and energy density of the modified pouch cells were carefully monitored and optimized.

The conservative estimation of the pouch cell energy densities revealed that by using the most advanced materials in the current literature related to RMB, it should be possible to reach a remarkable energy density approaching 160 W h kg^{-1}. Moreover, given the properties of the new chloride-free Mg borate-based electrolyte solutions, this can be enhanced further by utilizing high-voltage/capacity cathodes based on TMOs that were found active with Mg ions (*e.g.*, VO_x and MoO_x oxides). Therefore, through this work, we aim to emphasize the considerable but yet-to-be-realized potential of rechargeable magnesium batteries. We encourage further efforts to develop high-energy cathodes and thin Mg-alloy anodes and then to use more industrially relevant approaches to achieve cost-effective, sustainable, and environmentally friendly advanced chemistries for RMBs in the near future. A final important note is related to cycle life: achieving a prolonged cycle life is critically important for RMB that are supposed to be used for load leveling and large energy-storage applications. Although we did not address this critical aspect herein, thanks to the use of ethereal solutions, which are not reactive to Mg metal and cathodes which red-ox potentials do not challenge the anodic stability of the electrolyte solutions available today (<3 V *vs.* Mg), this goal may be achieved and well demonstrated in further studies of advanced RMB in the near future (extensive work is in progress by several groups throughout the world).

Author contributions

Rudi R. Maça: writing original draft, review and edit, conceptualization, investigation, methodology, calculations, formal analysis. J. Alberto Blázquez: conceptualization, methodology, supervision, review and edit, project administration, funding acquisition. Olatz Leonet and Ana Fernández-Barquín: investigation, supervision, review. Eneko Azaceta: investigation. Alexey Kovalevsky: AZ31 investigation, materials supply. Jean Frederic Martin and Dane Sotta: chevrel Phase cathode material supply. Zhirong Zhao-Karger and Zhenyou Li: boron-based electrolyte salt synthesis and supply. Yair Ein-Eli: solid-electrolyte part original draft, supervision. Doron Aurbach: conceptualization, supervision, writing, review and edit. Malachi Noked: conceptualization. Ayan Mukherjee, Aroa R. Mainar, Piotr Jankowski, Laurin Rademacher, Joachim Häcker, Sunita Dey, Siân E. Dutton, Sumana Kundu, Claire P. Grey, Rosa Palacin, Juan Maria García Lastra, Maximilian Fichtner contributed to the review and edit of the manuscript.

Conflicts of interest

There are no conflicts to declare.

Acknowledgements

This work was funded by European Union's Horizon 2020 research and innovation program under the FET Proactive call with grant agreement no 824066 *via* the "E-MAGIC" project.

Notes and references

1 S. Bobba, S. Carrara, J. Huisman, F. Mathieux, C. Pavel and I. European Commission. Directorate-General for Internal Market, Critical raw materials for strategic technologies and sectors in the EU: a foresight study.
2 J. Betz, G. Bieker, P. Meister, T. Placke, M. Winter and R. Schmuch, *Adv. Energy Mater.*, 2019, **9**, 1803170.
3 H. D. Yoo, I. Shterenberg, Y. Gofer, G. Gershinsky, N. Pour and D. Aurbach, *Energy Environ. Sci.*, 2013, **6**, 2265–2279.
4 D. A. J. Rand and P. T. Moseley, *Electrochemical Energy Storage for Renewable Sources and Grid Balancing*, Elsevier Inc., 2015, pp. 201–222.
5 J. W. Choi and D. Aurbach, *Nat. Rev. Mater.*, 2016, **1**, 16013.
6 European Commission, European Climate Law, The European Parliament and the Council of the European Union, Brussels, 2021.
7 D. Aurbach, Z. Lu, A. Schechter, Y. Gofer, H. Gizbar, R. Turgeman, Y. Cohen, M. Moshkovich and E. Levi, *Nature*, 2000, **407**, 724–727.
8 S. Kundu, N. Solomatin, Y. Kauffmann, A. Kraytsberg and Y. Ein-Eli, *Appl. Mater. Today*, 2021, **23**, 100998.
9 R. Mohtadi, O. Tutusaus, T. S. Arthur, Z. Zhao-Karger and M. Fichtner, *Joule*, 2021, **5**, 581–617.
10 A. Ponrouch and M. Rosa Palacín, *Philos. Trans. R. Soc., A*, 2019, **377**, 20180297.
11 V. Bhaghavathi Parambath, Z. Zhao-Karger, T. Diemant, M. Jäckle, Z. Li, T. Scherer, A. Gross, R. J. Behm and M. Fichtner, *J. Mater. Chem. A*, 2020, **8**, 22998–23010.

12 S. Chakrabarty, J. A. Blázquez, T. Sharabani, A. Maddegalla, O. Leonet, I. Urdampilleta, D. Sharon, M. Noked and A. Mukherjee, *J. Electrochem. Soc.*, 2021, **168**, 080526.
13 M. Matsui, *J. Power Sources*, 2011, **196**, 7048–7055.
14 R. Davidson, A. Verma, D. Santos, F. Hao, C. Fincher, S. Xiang, J. van Buskirk, K. Xie, M. Pharr, P. P. Mukherjee and S. Banerjee, *ACS Energy Lett.*, 2019, **4**, 375–376.
15 N. Bell, R. Waugh, D. Parker and K. Baker, *Magnesium Recycling in the EU*, 2017, pp. 1–79.
16 M. Fichtner, in *Royal Society of Chemistry*, ed. M. Fichtner, Royal Society of Chemistry, Ulm, 2019, pp. 1–16.
17 D. Aurbach, Z. Lu, A. Schechter, Y. Gofer, H. Gizbar, R. Turgeman, Y. Cohen, M. Moshkovich and E. Levi, *Nature*, 2000, **407**, 724–727.
18 S. Ferrari, M. Falco, A. B. Muñoz-García, M. Bonomo, S. Brutti, M. Pavone and C. Gerbaldi, *Adv. Energy Mater.*, 2021, **11**, 2100785.
19 M. A. Hannan, S. B. Wali, P. J. Ker, M. S. A. Rahman, M. Mansor, V. K. Ramachandaramurthy, K. M. Muttaqi, T. M. I. Mahlia and Z. Y. Dong, *J. Energy Storage*, 2021, **42**, 103023.
20 Z. Zhang, S. Shui and Z. Editors, *Green Energy and Technology Rechargeable Batteries Materials*, Technologies and New Trends, 2015.
21 A. Maddegalla, A. Mukherjee, J. A. Blázquez, E. Azaceta, O. Leonet, A. R. Mainar, A. Kovalevsky, D. Sharon, J. F. Martin, D. Sotta, Y. Ein-Eli, D. Aurbach and M. Noked, *ChemSusChem*, 2021, **14**, 4690–4696.
22 Y. Xiu, Z. Li, V. Bhaghavathi Parambath, Z. Ding, L. Wang, A. Reupert, M. Fichtner and Z. Zhao-Karger, *Batteries Supercaps*, 2021, **4**, 1850–1857.
23 R. Attias, M. Salama, B. Hirsch, Y. Goffer and D. Aurbach, *Joule*, 2019, **3**, 27–52.
24 T. D. Gregory, R. J. Hoffman and R. C. Winterton, *J. Electrochem. Soc.*, 1990, **137**, 775–780.
25 I. Shterenberg, M. Salama, Y. Gofer, E. Levi and D. Aurbach, *MRS Bull.*, 2014, **39**, 453–460.
26 C. B. Bucur, T. Gregory, A. G. Oliver and J. Muldoon, *J. Phys. Chem. Lett.*, 2015, **6**, 3578–3591.
27 I. Shterenberg, M. Salama, H. D. Yoo, Y. Gofer, J.-B. Park, Y.-K. Sun and D. Aurbach, *J. Electrochem. Soc.*, 2015, **162**, A7118–A7128.
28 R. Attias, B. Dlugatch, O. Blumen, K. Shwartsman, M. Salama, N. Shpigel and D. Sharon, *ACS Appl. Mater. Interfaces*, 2022, **14**, 30952–30961.
29 C. Liebenow, Z. Yang and P. Lobitz, *Electrochem. Commun.*, 2000, **2**, 641–645.
30 H. S. Kim, T. S. Arthur, G. D. Allred, J. Zajicek, J. G. Newman, A. E. Rodnyansky, A. G. Oliver, W. C. Boggess and J. Muldoon, *Nat. Commun.*, 2011, **2**, 427.
31 P. Wang and M. R. Buchmeiser, *Adv. Funct. Mater.*, 2019, **29**, 1905248.
32 R. E. Doe, R. Han, J. Hwang, A. J. Gmitter, I. Shterenberg, H. D. Yoo, N. Pour and D. Aurbach, *Chem. Commun.*, 2014, **50**, 243–245.
33 P. Canepa, S. Jayaraman, L. Cheng, N. N. Rajput, W. D. Richards, G. S. Gautam, L. A. Curtiss, K. A. Persson and G. Ceder, *Energy Environ. Sci.*, 2015, **8**, 3718–3730.
34 A. J. Crowe, K. K. Stringham and B. M. Bartlett, *ACS Appl. Mater. Interfaces*, 2016, **8**, 23060–23065.
35 Z. Zhao-Karger and M. Fichtner, *Front. Chem.*, 2019, **6**, 1–12.
36 J. Muldoon, C. B. Bucur, A. G. Oliver, J. Zajicek, G. D. Allred and W. C. Boggess, *Energy Environ. Sci.*, 2013, **6**, 482–487.
37 J. Song, E. Sahadeo, M. Noked and S. B. Lee, *J. Phys. Chem. Lett.*, 2016, **7**, 1736–1749.
38 Z. Zhao-Karger, R. Liu, W. Dai, Z. Li, T. Diemant, B. P. Vinayan, C. Bonatto Minella, X. Yu, A. Manthiram, R. J. Behm, M. Ruben and M. Fichtner, *ACS Energy Lett.*, 2018, **3**, 2005–2013.
39 Z. Zhang, Z. Cui, L. Qiao, J. Guan, H. Xu, X. Wang, P. Hu, H. Du, S. Li, X. Zhou, S. Dong, Z. Liu, G. Cui and L. Chen, *Adv. Energy Mater.*, 2017, **7**, 1602055.
40 F. Liu, T. Wang, X. Liu and L. Z. Fan, *Adv. Energy Mater.*, 2021, **11**, 2000787.
41 R. Mohtadi, M. Matsui, T. S. Arthur and S. J. Hwang, *Angew. Chem., Int. Ed.*, 2012, **51**, 9780–9783.
42 O. Tutusaus, R. Mohtadi, N. Singh, T. S. Arthur and F. Mizuno, *ACS Energy Lett.*, 2017, **2**, 224–229.
43 P. Canepa, G. Sai Gautam, D. C. Hannah, R. Malik, M. Liu, K. G. Gallagher, K. A. Persson and G. Ceder, *Chem. Rev.*, 2017, **117**, 4287–4341.
44 T. J. Carter, R. Mohtadi, T. S. Arthur, F. Mizuno, R. Zhang, S. Shirai and J. W. Kampf, *Angew. Chem., Int. Ed.*, 2014, **53**, 3173–3177.
45 Z. Zhao-Karger, M. E. Gil Bardaji, O. Fuhr and M. Fichtner, *J. Mater. Chem. A*, 2017, **5**, 10815–10820.
46 S. B. Son, T. Gao, S. P. Harvey, K. X. Steirer, A. Stokes, A. Norman, C. Wang, A. Cresce, K. Xu and C. Ban, *Nat. Chem.*, 2018, **10**, 532–539.
47 P. Jankowski, J. M. G. Lastra and T. Vegge, *Batteries Supercaps*, 2020, **3**, 1350–1359.
48 J. Drews, T. Danner, P. Jankowski, T. Vegge, J. M. García Lastra, R. Liu, Z. Zhao-Karger, M. Fichtner and A. Latz, *ChemSusChem*, 2020, **13**, 3599–3604.
49 J. Drews, P. Jankowski, J. Häcker, Z. Li, T. Danner, J. M. G. Lastra, T. Vegge, N. Wagner, K. A. Friedrich, Z. Zhao-Karger, M. Fichtner and A. Latz, *ChemSusChem*, 2021, **14**, 4820–4835.
50 M. Rashad, M. Asif, Y. Wang, Z. He and I. Ahmed, *Energy Storage Mater.*, 2020, **25**, 342–375.
51 Z. Zhao-Karger, R. Liu, W. Dai, Z. Li, T. Diemant, B. P. Vinayan, C. Bonatto Minella, X. Yu, A. Manthiram, R. J. Behm, M. Ruben and M. Fichtner, *ACS Energy Lett.*, 2018, **3**, 2005–2013.
52 N. Kamaya, K. Homma, Y. Yamakawa, M. Hirayama, R. Kanno, M. Yonemura, T. Kamiyama, Y. Kato, S. Hama, K. Kawamoto and A. Mitsui, *Nat. Mater.*, 2011, **10**, 682–686.
53 M. Guo, C. Yuan, T. Zhang and X. Yu, *Small*, 2022, **18**, 2106981.
54 P. W. Jaschin, Y. Gao, Y. Li and S. Bo, *J. Mater. Chem. A*, 2020, **8**, 2875–2897.

55 M. Wang, Z. Wang, S. Zhao, J. Wang and S. Wang, *Chin. J. Chem. Eng.*, 2017, **25**, 1581–1597.
56 R. Zhao, Y. Wu, Z. Liang, L. Gao, W. Xia, Y. Zhao and R. Zou, *Energy Environ. Sci.*, 2020, **13**, 2386–2403.
57 S. Ma, L. Shen, Q. Liu, W. Shi, C. Zhang, F. Liu, J. A. Baucom, D. Zhang, H. Yue, H. bin Wu and Y. Lu, *ACS Appl. Mater. Interfaces*, 2020, **12**, 43824–43832.
58 W. Xue, C. D. Sewell, Q. Zhou and Z. Lin, *Angew. Chem., Int. Ed.*, 2022, **61**, e2022065.
59 Y. Yoshida, K. Kato and M. Sadakiyo, *J. Phys. Chem. C*, 2021, **125**, 21124–21130.
60 B. Park and J. L. Schaefer, *J. Electrochem. Soc.*, 2020, **167**, 070545.
61 J. Sharma and S. Hashmi, *Polym. Compos.*, 2019, **40**, 1295–1306.
62 M. F. Bósquez-Cáceres, S. Hidalgo-Bonilla, V. Morera Córdova, R. M. Michell and J. P. Tafur, *Polymers*, 2021, **13**, 24.
63 K. M. Diederichsen, E. J. McShane and B. D. McCloskey, *ACS Energy Lett.*, 2017, **2**, 2563–2575.
64 P. Zhou, X. Zhang, Y. Xiang and K. Liu, *Nano Res.*, 2022, DOI: **10.1007/s12274-022-4833-1**.
65 Y. Pang, Y. Liu, J. Yang, S. Zheng and C. Wang, *Mater. Today Nano*, 2022, **18**, 100194.
66 J. Cuan, Y. Zhou, T. Zhou, S. Ling, K. Rui, Z. Guo, H. Liu and X. Yu, *Adv. Mater.*, 2019, **31**, 1803533.
67 A. H. Ahmad and F. S. A. Ghani, *AIP Conf. Proc.*, 2009, **1136**, 31–35.
68 Y. Gao, T. P. Mishra, S.-H. Bo, G. Sai Gautam and P. Canepa, *Annu. Rev. Mater. Res.*, 2022, **52**, 129–158.
69 P. Canepa, S.-H. Bo, G. Sai Gautam, B. Key, W. D. Richards, T. Shi, Y. Tian, Y. Wang, J. Li and G. Ceder, *Nat. Commun.*, 2017, **8**, 1759.
70 L.-P. Wang, Z. Zhao-Karger, F. Klein, J. Chable, T. Braun, A. R. Schür, C.-R. Wang, Y.-G. Guo and M. Fichtner, *ChemSusChem*, 2019, **12**, 2286–2293.
71 D. Hubble, D. E. Brown, Y. Zhao, C. Fang, J. Lau, B. D. McCloskey and G. Liu, *Energy Environ. Sci.*, 2022, **15**, 550–578.
72 K. Kisu, S. Kim, M. Inukai, H. Oguchi, S. Takagi and S. Orimo, *ACS Appl. Energy Mater.*, 2020, **3**, 3174–3179.
73 Y. Pang, Z. Nie, F. Xu, L. Sun, J. Yang, D. Sun, F. Fang and S. Zheng, *Energy Environ. Mater.*, 2022, e12527.
74 K. Kajihara, H. Nagano, T. Tsujita, H. Munakata and K. Kanamura, *J. Electrochem. Soc.*, 2017, **164**, A2183.
75 Y. Wang, Z. Liu, C. Wang, X. Yi, R. Chen, L. Ma, Y. Hu, G. Zhu, T. Chen, Z. Tie, J. Ma, J. Liu and Z. Jin, *Adv. Mater.*, 2018, **30**, 1802563.
76 M. Mao, T. Gao, S. Hou and C. Wang, *Chem. Soc. Rev.*, 2018, **47**, 8804–8841.
77 Z. Ma, D. R. MacFarlane and M. Kar, *Batteries Supercaps*, 2019, **2**, 115–127.
78 Q. Guo, W. Zeng, S. L. Liu, Y. Q. Li, J. Y. Xu, J. X. Wang and Y. Wang, *Rare Met.*, 2021, **40**, 290–308.
79 K. Jayasayee, R. Berthelot, K. C. Lethesh and E. M. Sheridan, *Magnesium Batteries: Research and Applications*, The Royal Society of Chemistry, 2020, pp. 114–141.
80 R. Attias, M. Salama, R. Pant, Y. Gofer and D. Aurbach, *J. Phys. Chem. C*, 2019, **123**, 16577–16587.
81 Y. Yang, X. Xiong, J. Chen, X. Peng, D. Chen and F. Pan, *J. Magnesium Alloys*, 2021, **9**, 705–747.
82 O. I. Malyi, T. L. Tan and S. Manzhos, *J. Power Sources*, 2013, **233**, 341–345.
83 T. Gao, S. Hou, K. Huynh, F. Wang, N. Eidson, X. Fan, F. Han, C. Luo, M. Mao, X. Li and C. Wang, *ACS Appl. Mater. Interfaces*, 2018, **10**, 14767–14776.
84 H. Dong, O. Tutusaus, Y. Liang, Y. Zhang, Z. Lebens-Higgins, W. Yang, R. Mohtadi and Y. Yao, *Nat. Energy*, 2020, **5**, 1043–1050.
85 R. Attias, M. S. Chae, B. Dlugatch, M. Oliel, Y. Goffer and D. Aurbach, *ACS Catal.*, 2020, **10**, 7773–7784.
86 D. Schloffer, S. Bozorgi, P. Sherstnev, C. Lenardt and B. Gollas, *J. Power Sources*, 2017, **367**, 138–144.
87 Z. Wu and W. A. Curtin, *Nature*, 2015, **526**, 62–67.
88 J. Niu, Z. Zhang and D. Aurbach, *Adv. Energy Mater.*, 2020, **10**, 2000697.
89 N. Singh, T. S. Arthur, C. Ling, M. Matsui and F. Mizuno, *Chem. Commun.*, 2013, **49**, 149–151.
90 K. Periyapperuma, T. T. Tran, M. I. Purcell and M. N. Obrovac, *Electrochim. Acta*, 2015, **165**, 162–165.
91 F. Murgia, E. T. Weldekidan, L. Stievano, L. Monconduit and R. Berthelot, *Electrochem. Commun.*, 2015, **60**, 56–59.
92 L. T. Ho, *Appl. Phys. Lett.*, 1979, **35**, 409–410.
93 T. S. Arthur, N. Singh and M. Matsui, *Electrochem. Commun.*, 2012, **16**, 103–106.
94 Z. Meng, D. Foix, N. Brun, R. Dedryvère, L. Stievano, M. Morcrette and R. Berthelot, *ACS Energy Lett.*, 2019, **4**, 2040–2044.
95 S. C. Jung and Y. K. Han, *J. Phys. Chem. C*, 2018, **122**, 17643–17649.
96 R. Mohtadi, O. Tutusaus, T. S. Arthur, Z. Zhao-Karger and M. Fichtner, *Joule*, 2021, **5**, 581–617.
97 K. Gusieva, C. H. J. Davies, J. R. Scully and N. Birbilis, *Int. Mater. Rev.*, 2015, **60**, 169–194.
98 J. Li, Y. Huang, F. Wang, X. Meng, L. Wan and Z. Dong, *Mater. Sci. Eng., A*, 2020, **773**, 138877.
99 W. Lu, L. Sun, Y. Zhao, T. Wu, L. Cong, J. Liu, Y. Liu and H. Xie, *Energy Storage Mater.*, 2021, **34**, 241–249.
100 S. Vincent, J. H. Chang and J. M. Garcia Lastra, *Batteries Supercaps*, 2021, **4**, 522–528.
101 J. Ma, G. Wang, Y. Li, C. Qin and F. Ren, *J. Mater. Eng. Perform.*, 2019, **28**, 2873–2880.
102 O. Chusid, Y. Gofer, H. Gizbar, Y. Vestfrid, E. Levi, D. Aurbach and I. Riech, *Adv. Mater.*, 2003, **15**, 627–630.
103 A. Pardo, M. C. Merino, A. E. Coy, F. Viejo, R. Arrabal and S. Feliú, *Electrochim. Acta*, 2008, **53**, 7890–7902.
104 G. L. Song, *JOM*, 2012, **64**, 671–679.
105 A. el Kharbachi, O. Zavorotynska, M. Latroche, F. Cuevas, V. Yartys and M. Fichtner, *J. Alloys Compd.*, 2020, **817**, 153261.
106 Z. Guo, S. Zhao, T. Li, D. Su, S. Guo and G. Wang, *Adv. Energy Mater.*, 2020, **10**, 1903591.
107 K. Tang, A. Du, S. Dong, Z. Cui, X. Liu, C. Lu, J. Zhao, X. Zhou and G. Cui, *Adv. Mater.*, 2020, **32**, 1904987.

108 E. Levi, A. Mitelman, D. Aurbach and M. Brunelli, *Chem. Mater.*, 2007, **19**, 5131–5142.
109 K. Lu, S. Gao, R. J. Dick, Z. Sattar and Y. Cheng, *J. Mater. Chem. A*, 2019, **7**, 6038–6044.
110 T. Koketsu, J. Ma, B. J. Morgan, M. Body, C. Legein, W. Dachraoui, M. Giannini, A. Demortière, M. Salanne, F. Dardoize, H. Groult, O. J. Borkiewicz, K. W. Chapman, P. Strasser and D. Dambournet, *Nat. Mater.*, 2017, **16**, 1142–1148.
111 Z. Li, B. P. Vinayan, P. Jankowski, C. Njel, A. Roy, T. Vegge, J. Maibach, J. M. G. Lastra, M. Fichtner and Z. Zhao-Karger, *Angew. Chem., Int. Ed.*, 2020, **59**, 11483–11490.
112 X. Chen, X. Wang, Z. Wang, W. Yu and Y. Qian, *Mater. Chem. Phys.*, 2004, **87**, 327–331.
113 C. Peng, H. Lyu, L. Wu, T. Xiong, F. Xiong, Z. Liu, Q. An and L. Mai, *ACS Appl. Mater. Interfaces*, 2018, **10**, 36988–36995.
114 R. Verrelli, A. P. Black, C. Frontera, J. Oro-Sole, M. E. Arroyo-De Dompablo, A. Fuertes and M. Rosa Palacín, *ACS Omega*, 2019, **4**, 8943–8952.
115 S. Dey, J. Lee, S. Britto, J. M. Stratford, G. Cibin, E. N. Keyzer, S. J. Cassidy, M. Elgaml, M. T. Dunstan and C. P. Grey, *J. Am. Chem. Soc.*, 2020, **142**, 19588–19601.
116 M. Vincent, V. S. Avvaru, M. C. Rodríguez, M. Haranczyk and V. Etacheri, *J. Power Sources*, 2021, **506**(1), 230118.
117 I. Gomez, O. Leonet, J. Alberto Blazquez, H. J. Grande and D. Mecerreyes, *ACS Macro Lett.*, 2018, **7**, 419–424.
118 B. Pan, J. Huang, Z. Feng, L. Zeng, M. He, L. Zhang, J. T. Vaughey, M. J. Bedzyk, P. Fenter, Z. Zhang, A. K. Burrell and C. Liao, *Adv. Energy Mater.*, 2016, **6**, 1600140.
119 K. Xu, *Chem. Rev.*, 2004, **104**, 4303–4418.
120 Q. Guo, W. Zeng, S. L. Liu, Y. Q. Li, J. Y. Xu, J. X. Wang and Y. Wang, *Rare Met.*, 2021, **40**, 290–308.
121 T. D. Gregory, R. J. Hoffman and R. C. Winterton, *J. Electrochem. Soc.*, 1990, **137**, 775–780.
122 A. Medina, C. Pérez-Vicente and R. Alcántara, *Materials*, 2021, **14**, 7488.
123 Y. Liang, R. Feng, S. Yang, H. Ma, J. Liang and J. Chen, *Adv. Mater.*, 2011, **23**, 640–643.
124 R. Demir-Cakan, M. R. Palacin and L. Croguennec, *J. Mater. Chem. A*, 2019, **7**, 20519–20539.
125 R. Y. Wang, C. D. Wessells, R. A. Huggins and Y. Cui, *Nano Lett.*, 2013, **13**, 5748–5752.
126 M. Liu, A. Jain, Z. Rong, X. Qu, P. Canepa, R. Malik, G. Ceder and K. A. Persson, *Energy Environ. Sci.*, 2016, **9**, 3201–3209.
127 H. D. Yoo, J. R. Jokisaari, Y. S. Yu, B. J. Kwon, L. Hu, S. Kim, S. D. Han, M. Lopez, S. H. Lapidus, G. M. Nolis, B. J. Ingram, I. Bolotin, S. Ahmed, R. F. Klie, J. T. Vaughey, T. T. Fister and J. Cabana, *ACS Energy Lett.*, 2019, **4**, 1528–1534.
128 G. Sai Gautam, P. Canepa, A. Abdellahi, A. Urban, R. Malik and G. Ceder, *Chem. Mater.*, 2015, **27**, 3733–3742.
129 R. Verrelli, A. P. Black, C. Pattanathummasid, D. S. Tchitchekova, A. Ponrouch, J. Oró-Solé, C. Frontera, F. Bardé, P. Rozier and M. R. Palacín, *J. Power Sources*, 2018, **407**, 162–172.
130 S. Dey, J. Lee, S. Britto, J. M. Stratford, E. N. Keyzer, M. T. Dunstan, G. Cibin, S. J. Cassidy, M. Elgaml and C. P. Grey, *J. Am. Chem. Soc.*, 2020, **142**, 19588–19601.
131 Z. Li, S. Ding, J. Yin, M. Zhang, C. Sun and A. Meng, *J. Power Sources*, 2020, **451**, 227815.
132 C. S. Rout, B. H. Kim, X. Xu, J. Yang, H. Y. Jeong, D. Odkhuu, N. Park, J. Cho and H. S. Shin, *J. Am. Chem. Soc.*, 2013, **135**, 8720–8725.
133 P. Gressier, I. Myung-hwan Whangbo, C. Alain Meerschaut and J. Rouxell, *Inorg. Chem.*, 1984, **23**, 1221–1228.
134 I. P. Batra, *Phys. Rev. B: Condens. Matter Mater. Phys.*, 1990, **42**, 9162–9165.
135 H. Dong, Y. Liang, O. Tutusaus, R. Mohtadi, Y. Zhang, F. Hao and Y. Yao, *Joule*, 2019, **3**, 782–793.
136 M. Kirchhöfer, J. von Zamory, E. Paillard and S. Passerini, *Int. J. Mol. Sci.*, 2014, **15**, 14868–14890.
137 F. J. Günter, C. Burgstaller, F. Konwitschny and G. Reinhart, *J. Electrochem. Soc.*, 2019, **166**, A1709–A1714.
138 H. Li, *Joule*, 2019, **3**, 911–914.
139 S. Dörfler, H. Althues, P. Härtel, T. Abendroth, B. Schumm and S. Kaskel, *Joule*, 2020, **4**, 539–554.
140 S. Chen, C. Niu, H. Lee, Q. Li, L. Yu, W. Xu, J. G. Zhang, E. J. Dufek, M. S. Whittingham, S. Meng, J. Xiao and J. Liu, *Joule*, 2019, **3**, 1094–1105.
141 D. Karabelli and K. P. Birke, *Appl. Sci.*, 2021, **11**, 7592.
142 P. Saha, M. K. Datta, O. I. Velikokhatnyi, A. Manivannan, D. Alman and P. N. Kumta, *Prog. Mater. Sci.*, 2014, **66**, 1–86.
143 K. Itaoka, I. T. Kim, K. Yamabuki, N. Yoshimoto and H. Tsutsumi, *J. Power Sources*, 2015, **297**, 323–328.
144 Z. Li, T. Diemant, Z. Meng, Y. Xiu, A. Reupert, L. Wang, M. Fichtner and Z. Zhao-Karger, *ACS Appl. Mater. Interfaces*, 2021, **13**, 33123–33132.
145 J. Hao, F. Yang, S. Zhang, H. He, G. Xia, Y. Liu, C. Didier, T. Liu, W. K. Pang, V. K. Peterson, J. Lu and Z. Guo, *Des. Res.*, 2020, **117**, 2815–2823.
146 M. S. E. Houache, C. H. Yim, Z. Karkar and Y. Abu-Lebdeh, *Batteries*, 2022, **8**(7), 70.
147 Z. Zhao-Karger, R. Liu, W. Dai, Z. Li, T. Diemant, B. P. Vinayan, C. Bonatto Minella, X. Yu, A. Manthiram, R. J. Behm, M. Ruben and M. Fichtner, *ACS Energy Lett.*, 2018, **3**, 2005–2013.